Heat exchanger design and performance evaluation for a high-temperature heat pump system under different two-phase correlations: 4E analysis

Applied Energy 384 (2025) 125492

Contents lists available at ScienceDirect

Applied Energy

journal homepage: www.elsevier.com/locate/apenergy

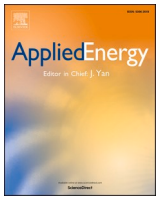

Heat exchanger design and performance evaluation for a high-temperature heat pump system under different two-phase correlations: 4E analysis

Ding Wu [a], Bo Ma [a,*], Xiaohui Huang [a], Xian Wu [b], Yan Yang [c], Chuang Wen [d,*], Ji Zhang [a,d]

[a] School of Electrical and Information Engineering, Hunan University, Changsha, 410082, China
[b] Shenzhen Tianjian Engineering Technology Co., Ltd., Shenzhen, 518109, China
[c] Faculty of Environment, Science and Economy, University of Exeter, Exeter, EX4 4QF, UK
[d] School of the Built Environment, University of Reading, Reading RG6 6AH, UK

HIGHLIGHTS

- A comparative analysis among 8 two-phase heat transfer correlations was conducted.
- Correlations impacted the designed condensers more significantly than evaporators.
- Heating capacity were notably influenced, with a relative difference of 9.88 %.
- Heating costs varied minimally, showing a relative difference of 1.91 %.
- Total carbon emissions remained largely changed, with a relative difference of 6.38 %.

ARTICLE INFO

Keywords:
Heat pump
Plate heat exchanger
Two-phase correlation
4E analysis
Energy Storage
High-temperature Heat Pump

ABSTRACT

Supplying district heat and assisting the integration of renewable electricity, high-temperature heat pump technology is foreseen to play an essential role in renewable energy-powered thermal energy storage systems. However, existing studies on high-temperature heat pump performance prediction are usually based on utilizing specific heat transfer correlations of heat exchangers. It is difficult to guide the selection and combination of the two-phase correlations in the heat exchanger design and system performance assessment of the high-temperature heat pump. In the present study, we aim to focus on the impact of different two-phase correlations, and a comparative study is conducted among 8 correlations (4 flow condensation ones and 4 flow boiling ones) adopted for component design and system performance prediction. The results show that for designed condensers or evaporators, the dimensions, costs, and carbon emissions are significantly affected by different two-phase correlations. Among 16 pairs of two-phase correlations, little fluctuation of the system performance is observed at the design heat source temperature 80 °C. While at off-design heat source temperatures of 85, 90 or 95 °C, the energetic and exergetic performance parameters are significantly affected with high relative differences (9.88% of heating capacity, 3.27% of coefficient of performance, and 6.76% of exergy efficiency). Also, the system's economic and environmental performance indexes are influenced to some extent, with visible relative uncertainties (1.91% of the heating cost, 4.44% of the payback time, and 6.38% of the carbon emission). This research will help to promote the selection and utilization of two-phase correlations for the plate heat exchanger design and system assessment in larger renewable energy-powered high-temperature heat pump applications.

1. Introduction

With the widespread use of fossil fuels in the process of industrial society and global economic development, a series of global warming issues such as air pollution, global temperature rise, and glacier melting have become increasingly severe, posing a serious threat to the living environment of humanity [1]. Recently, a comprehensive roadmap "net-zero emission by 2050" has been released by the IEA (International Energy Agency) [2], which mentioned that from 2030 to 2050 the global proportion of energy-saving heating technologies including the heat pump (HP) as alternatives of natural gas heating, needs to increase from

* Corresponding author.
E-mail addresses: boma@hnu.edu.cn (B. Ma), c.wen@reading.ac.uk (C. Wen).

https://doi.org/10.1016/j.apenergy.2025.125492
Received 29 December 2024; Received in revised form 25 January 2025; Accepted 4 February 2025
Available online 13 February 2025

Nomenclature

Abbreviations

HP	Heat pump
OM	Operation and maintenance
LCCP	Life Cycle Climate Performance
NSGA-II	Nondominated sorting genetic algorithm II
PHE	Plate heat exchanger
COP	Coefficient of performance
GWP	Global Warming Potential
ODP	Ozone Depletion Potential
TCI	Total capital investment
PEC	Purchased equipment cost

Variables

A	Heat transfer area (m^2)
AEC	Annual electricity consumption (kW·h)
ALR	Annual refrigerant leakage proportion (−)
Bo	Boiling number (−)
b	Plate corrugation depth (mm)
CF	Cash flow(€)
Co	Convection number (−)
CRF	Capital recovery factor(−)
c	Cost(€)
Em	Emission value of CO_2 (t)
EOL	Refrigerant leakage ratio at the end of life (−)
Fr	Froude number (−)
f	Correction coefficient (−)
G	Mass flux ($kg/(s·m^2)$)
Ge	Geometric parameters (−)
g	Gravitational acceleration (m/s^2)
h	Enthalpy (kJ/kg)
i_{eff}	Effective interest rate (−)
k	Thermal conductivity (W/(m·°C))
L	Length (m)
M	Molar mass (g/mol)
μ	Dynamic viscosity (Pa·s)
c_p	Constant pressure specific heat capacity (kJ/(kg·°C))
τ	Compressor pressure ratio (−)
ρ	Density (kg/m^3)
σ	Surface tension (N)
m	Mass flow (kg/s)
Nu	Nusselt number (−)
n	lifetime of equipment (year)
Pr	Prandtl number (−)
p	Pressure (kPa)
Q	Heat transfer rate (kW)
q	Heat flux, (kW/m^2)
x	Vapor quality (−)

Superscript and subscript

ave	Average
comp	Compressor
cond	Condenser
crit	Critical
des	Destruction
el	Electricity consumption
ip	Inlet port
eva	Evaporator
c	Heat sink
m	Mean
h	Heat source
op	Outlet port
pool	Pool boiling
pp	Pinch point
sp	Single-phase
sup	Superheated
tp	Two-phase
tv	Throttle valve
v	Vapor
w	Working fluid
wall	Wall surface
Δ	Difference
x	Iteration variable

nearly 20% to around 55% [3]. With an average electric heating conversion efficiency of almost 300%, HP is a promising type of high-efficiency and energy-saving technology for building heating [4]. As is well known, traditional heating equipment such as fuel-fired boilers [5] or direct electric heating facilities [6] has been widely installed and utilized, which have relatively low energy efficiency, leading to serious energy waste and a large amount of carbon emissions. For this reason, many governments have set ambitious emission reduction targets such as the German Federal Government [7] which is now launching a comprehensive push for the residential heating equipment transformation into the heat pump.

Through steam compression thermodynamic cycles, HP realizes the thermal energy transfer from an available renewable heat resource [8,9] or waste heat from processing industries [10] to a high-temperature heat sink, which expands the thermal energy utilization range of low-grade heat. Particularly when powered by intermittent renewable electricity [11], HP based thermal energy storage system is environmentally friendly for building heating and is beneficial to reduce the demand for traditional fossil fuels and carbon emissions. Therefore, integrated with low-cost heat sources (e.g. geothermal [12], solar thermal [13] or industrial waste heat [14]), HP based thermal energy storage system for residential heating with high renewable electricity energy penetration has received widespread attention in recent years [15,16]. Lee et al. [17] achieved a 62% improvement in the energy efficiency of thermal energy storage systems by optimizing the operation of the heat pump subsystems and thermal storage tanks. Sakellariou et al. [18] identified that the capacity of the storage tank and the efficiency of the heat exchangers in the heat pump subsystem are the most influential factors affecting the thermal performance of heat pump storage systems. The temperature distribution within the plate heat exchanger which is a critical component of the heat pump subsystem, has a significant impact on the coefficient of performance of the heat pump cycle, reaching up to 48.7% [19]. Liu et al. [20] found that the design dimensions of plate heat exchangers in ground source heat pump systems play a crucial role in the economic performance of the system. Marinelli et al. [21] assessed the environmental impact of heat pump systems, concluding that the production of plate heat exchangers constitutes a significant portion of the environmental impact indicators of heat pump systems.

As the most important electrothermal conversion unit, HP performs a crucial role in the entire thermal energy storage system and abundant research has been devoted to its performance enhancement [22]. Numerous studies concluded in common that the heat exchanger constitutes the most significant portion of the overall capital expenditure in heat pump systems, often reaching up to 70% [23], and it also has the most obvious impact on the system operation performance [24,25]. Therefore, optimizing the design of the heat exchanger holds paramount importance in the process of enhancing heat pump system efficiency. Among the diverse array of heat exchanger configurations, the plate-type design is extensively employed within the realm of heat pumps because of its notable advantages such as simplicity in assembly/

disassembly, high efficiency, and easy maintainability [26]. In order to accurately forecast the performance of plate-type heat exchangers (PHEs) and subsequently assess the overall system efficiency of heat pumps, a range of heat transfer correlations have been formulated and widely utilized [27]. Different correlations involve various refrigerants and experimental conditions, each with specific applicability and limitations [28]. Additionally, the derivation methods of different correlations vary, such as direct fitting of abundant experimental data [29], statistical analysis through multivariable regression [30], and improvements based on existing correlations [31]. Therefore, only a subset of correlations is adopted in this study for comparative analysis.

From the perspective of correlations adopted in heat pump system simulations, 8 two-phase heat transfer correlations (4 flow boiling ones proposed by Amalfi et al. [32], Yan and Lin [33], Zhang and Haglind [34], and Liu and Winterton [29]; 4 flow condensation ones suggested by Zhang et al. [35], Kuo et al. [36], Han et al. [37], and Yan et al. [38]) have been picked out in this paper due to their mature utilization. The choice to exclude the latest heat transfer correlations was driven by the consideration that their reliability and general applicability are not yet fully verified. To maintain scientific rigor and facilitate meaningful comparisons, this study focused on established correlations that have been extensively validated and are widely recognized in the context of vapor compression heat pump cycles and other thermodynamic applications. The characteristics and distinctions among them are summarized and listed in Table 1. And a significant volume of research has been conducted utilizing the aforementioned 8 correlations. On the one hand, for an independent heat pump system, Kim et al. [39] obtained a satisfactory coefficient of performance (COP) through optimization of heat exchanger design parameters. A transient model of a residential heat pump was proposed by Salazar-Herran et al. [40] for the mode-switching characteristic analysis between cooling and heating. A techno-economic comparison analysis between R1234ze(E) and R134a heat pumps was conducted by Yan et al. [41] and R1234ze(E) showed economic advantages compared with R134a. A comprehensive analysis of four hydrocarbon working fluids for a heat pump system, considering both thermo-economic and environmental factors, was conducted by Zhao et al. [42] and R600 was considered to be a highly promising choice. On the other hand, for the heat pump unit integrated into a larger energy utilization system, Fischer et al. [43] discussed the optimal control strategy of a heat pump unit for the accommodation of photovoltaic electricity generation. In order to improve the utilization efficiency of the constrained electric energy discharged from vehicle batteries, effective thermal management strategies for the electric vehicle heat pump units have been developed, considering the recovery heat sources from electric devices [44], from air-to-air regenerative heat exchangers [45], or from the fuel cell and battery units [46]. In other heat pump utilization cases, abundant thermo-economic assessments have also been carried out, e.g. the industrial heat pump of MW level [47], the heat pump designed for marine waste heat recovery [48], and the residential heat pump for air/ground-source thermal integration [49].

Over the past decade, among the existing studies [39–49] related to heat exchanger design and heat pump system performance optimization, a specific two-phase correlation was often selected and applied for predicting heat transfer performance behaviors of heat exchanger components. It is worth emphasizing that various correlations are derived from distinct experimental data under different operation conditions or working fluids. In this study, the correlations referenced in these prior works [39–49] have been thoroughly examined and utilized as a foundation to systematically analyze the potential predictive variations among different correlations. This approach ensures that the selected correlations provide a robust and representative basis for comprehensive comparative analysis. Hence, in the design process of heat exchanger components or during the performance assessment of heat pump systems, it's worth noting that the predicted results under the same boundary conditions may exhibit variations when using different two-phase correlations. Two-phase flows involve the simultaneous flow of two different phases of matter, typically liquid and vapor, as seen in boiling or condensation processes. In this study, the term 'correlation combinations' refers to the use of various empirical or semi-empirical correlations employed by engineers to calculate key parameters such as heat transfer coefficients and pressure drops across heat exchangers in two-phase flow conditions." To the authors' knowledge, there is a lack of similar reference literature available for comparing and analyzing the diversity and variation in the predicted performance of heat pump systems using different correlation combinations. However, diverse heat transfer prediction results by different correlation combinations would result in deviations in the dimension parameters of designed heat exchangers and further lead to different performance assessment outcomes of the whole heat pump system, which would definitely influence the

Table 1
Characteristics of the adopted 8 two-phase heat transfer correlations.

Ref.	Authors	Characteristics	Major Contributions	Year
[32]	Amalfi et al.	Conducted sensitivity analysis of existing prediction methods, clarified the impact of geometry on thermo-hydraulic performance	Developed new prediction methods for heat transfer and pressure drop, providing more reliable tools for optimizing plate heat exchanger design	2016
[33]	Yan and Lin	Studied the effect of vapor quality on evaporation heat transfer and pressure drop, especially at high vapor quality	Proposed empirical correlations for the evaporation heat transfer coefficient and friction factor for refrigerant R-134a	1999
[34]	Zhang and Haglind	Investigated the performance of seven working fluids under different reduced pressures and mass fluxes at high temperatures	Provided extensive experimental data on high-temperature flow boiling, developed methods for predicting frictional pressure drops	2021
[29]	Liu and Winterton	Proposed a general correlation based on the nucleate pool boiling equation for predicting heat transfer coefficients in tubes	Provided a more broadly applicable prediction tool compared to existing methods	1991
[35]	Zhang et al.	Covered heat transfer and pressure drop characteristics over a temperature range of 30 °C to 70 °C	Provided extensive experimental data on condensation heat transfer and pressure drop, developed a new correlation	2019
[36]	Kuo et al.	Investigated the condensation heat transfer and frictional pressure drop characteristics of R-410A in vertical plate heat exchangers	Proposed empirical correlations for predicting the condensation heat transfer coefficient of R-410A	2005
[37]	Han et al.	Studied the condensation heat transfer and pressure drop characteristics of R410A and R22 with different Chevron angles	Proposed correlations for Nusselt number and friction factor based on geometric parameters	2003
[38]	Yan et al.	Investigated the condensation heat transfer and frictional pressure drop characteristics of R-134a in vertical plate heat exchangers	Proposed correlations for predicting the condensation heat transfer coefficient of R-134a	1998

researchers' judgment. The effect of choosing different correlation combinations on the heat pump system performance has not been thoroughly explored so far.

In the context of geothermal-integrated heat pump energy storage systems, this study conducts a performance assessment and comprehensive comparative analysis of heat pump systems under sixteen different correlation pairs using eight distinct correlations (four for evaporation and four for condensation) based on the 4E analysis method [50]. This study consists of three sequential parts: first, a multi-objective thermo-economic optimization for working fluid screening is conducted from 11 candidates to select a suitable refrigerant fluid and obtain the corresponding optimal working condition. Second, regarding the obtained working condition as the heat exchanger design condition, the influence of various correlations is discussed from the dimension, economic and environmental performance. Third, the impact of 16 pairs of various correlation combinations on the system performance is investigated to uncover the underlying relationships between different correlations and changes in heat pump performance indicators. The component exergy destruction rates and system exergy efficiencies are presented for comparative analysis. Among various correlation pairs, the levelized specific cost of heat (c_h) and the payback time (*PBT*) are compared in economic analysis and the LCCP (Life Cycle Climate Performance) assessment method is applied in environmental analysis. This work seeks to demonstrate the influence of different two-phase correlations on the comprehensive performance assessment of a heat pump system, offering valuable insights for the plate heat exchanger design and the heat pump system development.

2. Methods

2.1. System description

An HP-based thermal energy storage system for renewable electricity utilization has attracted attention worldwide recently because of its low maintenance cost, high reliability, convenient operation, high compactness and environmental friendliness [12,51]. The fundamental framework of a such system could be illustrated in Fig. 1 [52]. The direction of energy flow is indicated by the arrows in Fig. 1, where surplus electricity generated from wind, solar, or thermal power plants is conveyed to the compressor of the geothermal heat pump unit. Subsequently, the compressors, driven by electricity, are utilized to enhance the grade of geothermal energy absorbed from the evaporator, with the higher-temperature heat energy either directly delivered by the condenser to centralized heating users or stored for later use. This process enables environmentally friendly and low-carbon centralized ground source heat pump heating. Both the evaporator and condenser investigated in this paper are supposed to be plate heat exchangers which are designed via various flow boiling or condensation correlations (4 flow boiling ones proposed by Amalfi et al. [32], Yan and Lin [33], Zhang and Haglind [34], and Liu and Winterton [29]; 4 flow condensation ones suggested by Zhang et al. [35], Kuo et al. [36], Han et al. [37], and Yan et al. [38]). On the basis of geothermal heat pumps, renewable electricity or grid peak power can be utilized and transferred into thermal energy, after which the generated heat would be stored or transmitted for district heating. Considering that a higher temperature level is more conducive to electricity generation rather than heat utilization [53], the initial assumption for the geothermal temperature is set at 80 °C as the heat source of the heat pump system. A heat pump system, as depicted in Fig. 2 (a), is fundamentally comprised of 4 components (a compressor, a throttle valve, a condenser, and an evaporator). The HP cycle *T-s* diagram is presented intuitively by the state points marked in detail, as shown in Fig. 2 (b).

To simplify and facilitate the simulation of the HP system, following assumptions are made in this article [49]. Notably, the pinch point temperature difference assumption in this study implies constant heat transfer coefficients across different phase regions and flow mediums in plate heat exchangers. This approach is adopted to facilitate the simplified dimensioning of heat exchangers, as thoroughly discussed in Ref. [54].

(1) Operation of the system is under stable conditions;
(2) Pressure drop is ignored across all the pipelines and components;
(3) No heat loss is assumed for the components and pipelines.
(4) An isenthalpic throttling process is considered in the expansion valve.

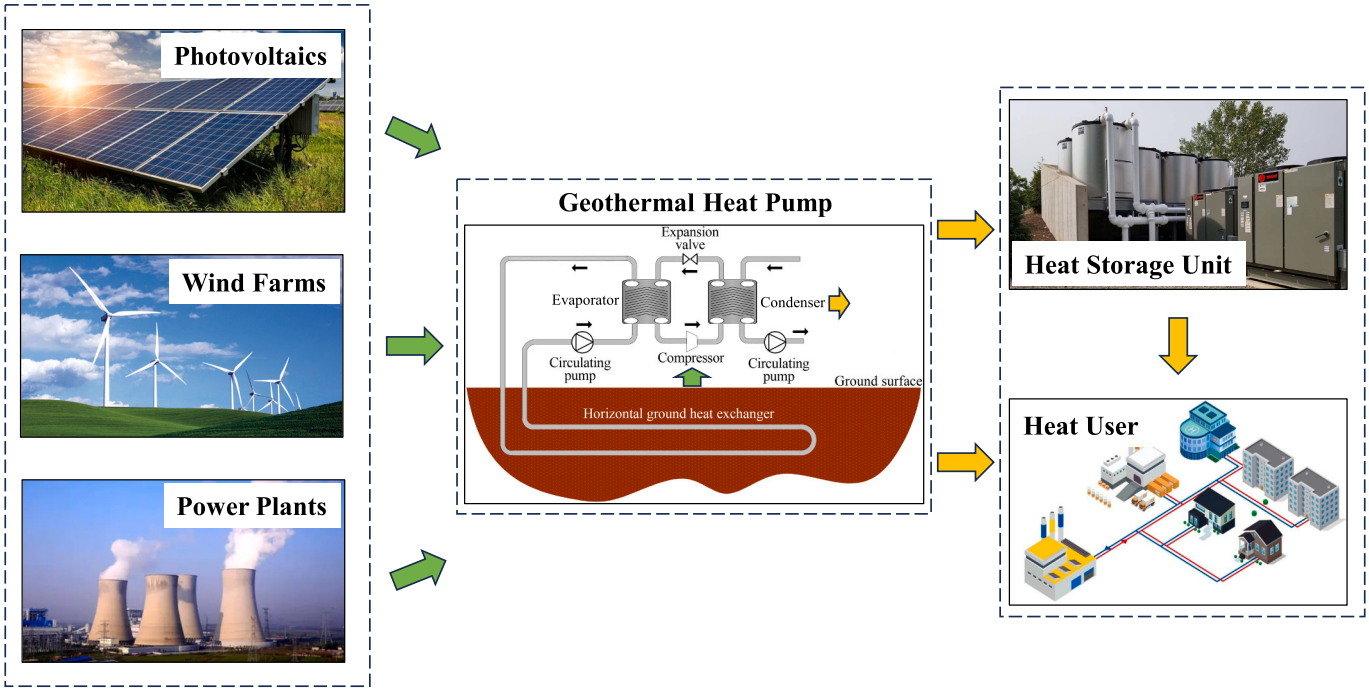

Fig. 1. Application background of the HP-based thermal energy storage system [52].

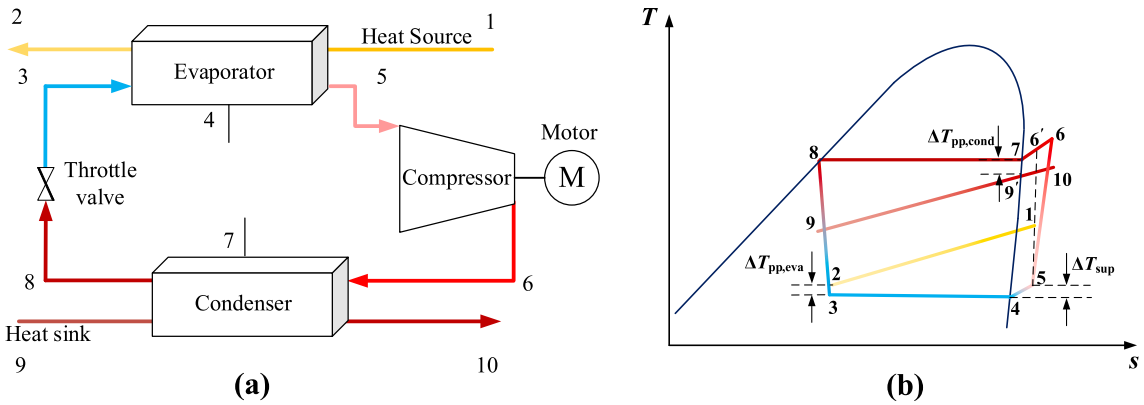

Fig. 2. (a) The fundamental structure of HP, (b) The cycle *T-s* diagram.

Given the assumptions mentioned above, the fundamental mathematical description of the HP system is detailed by following equations. For the evaporator, the pinch point illustrated in Fig. 2 (b) $\Delta T_{pp,eva}$ is calculated by:

$$\Delta T_{pp,eva} = T_2 - T_3 \tag{1}$$

The superheat degree is calculated by:

$$\Delta T_{sup} = T_5 - T_4 \tag{2}$$

With no heat loss, the heat transfer rate Q_{eva} is obtained by:

$$Q_{eva} = m_h(h_1 - h_2) = m_f(h_5 - h_3) \tag{3}$$

where m_h and m_f denote the mass flow rates of the heat source medium and the working fluid respectively.

For the condenser, marked in Fig. 2 (b), the pinch point of the condenser $\Delta T_{pp,cond}$ is defined as:

$$\Delta T_{pp,cond} = T_7 - T_{9'} \tag{4}$$

The heating capacity Q_{cond} is gained through:

$$Q_{cond} = m_f(h_6 - h_8) = m_c(h_{10} - h_9) \tag{5}$$

where m_c denotes the mass flow rate of the heat sink medium.

As a constraint for the operation reasonability of the compressor, the pressure ratio τ,is assumed to be in the range of 2 to 10, which is listed in Table 2. The compressor isentropic efficiency η_{comp} is:

$$\eta_{comp} = (h_{6'} - h_5)/(h_6 - h_5) \tag{6}$$

The consumed electrical power of the compressor W_{comp} is illustrated as:

$$W_{comp} = m_f(h_6 - h_5)/\eta_{mech}\eta_{gene} \tag{7}$$

where η_{mech} and η_{gene} represent the mechanical efficiency and generating efficiency respectively, which are calculated as Eq. 8 and Eq. 9 according to Ref. [55]. It should be noted that t_u and t_s are the absolute temperature of the hot and cold source, which are 110 °C and 80 °C respectively; Δt_c is the temperature difference between the condensation temperature and the hot source temperature which is considered as the pinch point of 2 °C; Δt_0 is the temperature difference between the cold source temperature and the evaporation temperature which is also considered as the pinch point of 2 °C; and Q_{hp} is the thermal power of the HP which is assumed as 3 MW averagely. And the final pre-defined values of η_{mech} and η_{gene} are listed in Table 2.

$$\eta_{mech} = 0.85 + 0.158Q_{hp}/\{1.16Q_{hp} + 0.1513(t_u + \Delta t_c)/[(t_u + \Delta t_c) - (t_s - \Delta t_0)]\} \tag{8}$$

$$\eta_{gene} = 0.85 + 0.139Q_{hp}/\{1.335Q_{hp} + 0.0904(t_u + \Delta t_c)/[(t_u + \Delta t_c) - (t_s - \Delta t_0)]\} \tag{9}$$

The isenthalpic process in the throttle valve is described as:

$$h_8 = h_3 \tag{10}$$

The assumed value for the aforementioned boundary condition parameters of the system is displayed in Table 2. To expand the usage range of the thermal energy stored by the pressurized water at 5 bars, a heat sink outlet temperature of 110 °C is assumed. And the temperature dropping or lifting is fixed as 30 °C with the initial geothermal source temperature of 80 °C. In addition, the evaporator heat transfer rate Q_{eva} is assumed as 2 MW [56].

Table 2
The assumed HP cycle parameters.

Cycle parameter	Symbol	Value	Unit
heat sink inlet temperature	$T_{c,ip}$	80	°C
heat sink outlet temperature	$T_{c,op}$	110	°C
heat sink fluid pressure	p_c	5	bar
superheating degree	T_{sup}	5	°C
pinch point	ΔT_{pp}	2	°C
condenser outlet steam quality	$q_{cond,op}$	0	–
heat source inlet temperature	$T_{h,ip}$	80	°C
heat source outlet temperature	$T_{h,op}$	50	°C
heat source fluid pressure	p_h	1	bar
compressor isentropic efficiency	η_{comp}	80	%
compressor volumetric efficiency	$\eta_{v,\ comp}$	90	%
mechanical efficiency	η_{mech}	98.62	%
generating efficiency	η_{gene}	95.41	%
compressor pressure ratio	τ	2 to 10	–
evaporator heat transfer rate	Q_{eva}	2	MW

2.2. Multi-objective optimization model for working fluid screening

2.2.1. Working fluid candidates

Prior to the introduction of the multi-objective optimization model, the preliminary selection of the candidate working fluids is conducted. The profound influence of refrigerant selection on the heat pump system performance has been emphasized in numerous previous studies [50,57]. As a result, choosing suitable working fluids from the extensive array of available refrigerants is a critical initial step. Safety considerations prefer those fewer attributes, such as flammability or toxicity, may be present. As listed in Table 3, The SG (Safety Grade) value of A1 implies that the flammability level is A and the toxicity level is 1. Additionally, it is imperative that the selected working fluids demonstrate minimal detrimental effects on the ozone layer or contribution to a low greenhouse effect. In quantitative terms, an ODP (Ozone Depletion Potential) value below 0.05 or a GWP (Global Warming Potential) value less than 1 is deemed desirable and highly acceptable. Abiding by these

Table 3
The properties of candidate fluids for screening.

Refrigerant	Molecular formula	T_{crit}/°C	P_{crit}/bar	ODP	GWP_{100}	SG	NBP/°C	MW/g·mol^{-1}
R600	C_4H_8	152.0	38.0	0	4	A3	−0.5	58.1
R600a	C_4H_{10}	134.7	36.3	0	3	A3	−11.8	58.1
R114	$C_2Cl_2F_4$	145.7	32.2	0.6	3.7	A1	3.5	170.9
R124	C_2HClF_4	122.3	35.9	0.026	620	A1	−12.0	136.5
R236ea	$C_3H_2F_6$	139.3	33.9	0	0.63	A1	6.1	152.0
R236fa	$C_3H_2F_6$	124.9	31.7	0	6300	A1	−1.6	152.0
R245fa	$C_3H_3F_5$	154.0	36.1	0	1030	B1	15.1	134.0
R1234ze(Z)	$C_3H_2F_4$	150.1	35.3	0	<1	A2L	9.8	114.0
R1234ze(E)	$C_3H_2F_4$	109.4	36.4	0	<1	A2L	−19.0	114.0
R1233zd(E)	$C_3H_2ClF_3$	166.5	36.2	0.00034	1	A1	18.0	130.5
R1224yd(Z)	C_3HClF_4	155.5	33.3	0.00012	<1	A1	14.0	148.5

abovementioned criteria, and considering the feasible subcritical temperature range, a total of 11 refrigerant fluids have been identified as candidates. A list of the candidate fluids is presented and detailed in Table 3.

where SG, NBP and MW denote the safety grade, normal boiling point and molecular weight of the refrigerant respectively.

2.2.2. Multi-objective optimization method

The enhanced version of the genetic algorithm known as the Non-dominated Sorting Genetic Algorithm II (NSGA-II) was proposed by Deb et al. [58], which demonstrates an excellent capability and offers fast solutions efficiently. In an effort to comprehensively assess and compare the HP system thermo-economic performance among the 11 working fluid candidates, NSGA-II is utilized to search for the Pareto frontiers. These obtained frontiers represent the optimal comprehensive performance points and comprise the corresponding working conditions for each candidate working fluid. In the optimization procedure, the decision variables are set as the evaporation pressure (p_{eva}) and condensation pressure (p_{cond}).

It is evident that the p_{eva} is typically maintained at levels less than 0.4 times the refrigerant critical pressure (p_{crit}) [41,59,60], and the p_{cond} is consistently several times that of p_{eva} [61,62]. Hence, in order to maximize the population size under a reasonable range and improve the rationality of the optimization results, the variation ranges of p_{cond} and p_{eva} are set as 0.5–0.9 p_{crit} and 0.01–0.4 p_{crit} respectively. As for the optimization objectives, the coefficient of performance *COP*, the exergy efficiency η_{II}, the cost of heat c_h and the payback time *PBT* are picked up respectively as energy, exergy and economic performance evaluation indexes.

As a sorting method for multi-objective sets, technique for order preference by similarity to ideal solution (TOPSIS) is widely used in the existing research especially for the sorting of Pareto frontiers [63]. The mathematical description of this sorting method is illustrated as follows:

First, an m × n decision matrix is defined by m working conditions and n indicators in the Pareto frontiers:

$$Y = \left(y_{ij}\right)_{m\times n} = \begin{pmatrix} y_{11} & y_{21} & \cdots & y_{1n} \\ y_{21} & y_{22} & \cdots & y_{2n} \\ \vdots & \vdots & \vdots & \vdots \\ y_{m1} & \vdots & \cdots & y_{mn} \end{pmatrix} \tag{11}$$

where y_{ij} means the numerical size of the *j*-th indicator under the *i*-th working condition.

To eliminate the effect of magnitude difference among various indicators, a normalization process is conducted by:

$$y_j^+ = \max_{i=1,2,\ldots,m}\left(y_{i1}, y_{i2}, \ldots, y_{ij}\right), j = 1, 2, \ldots, n \tag{12}$$

$$y_j^- = \min_{i=1,2,\ldots,m}\left(y_{i1}, y_{i2}, \ldots, y_{ij}\right), j = 1, 2, \ldots, n \tag{13}$$

$$e_{ij} = \left(y_{ij} - y_j^-\right) \Big/ \left(y_j^+ - y_j^-\right), j = 1, 2, \ldots, n \tag{14}$$

$$e_{ij} = \left(y_j^+ - y_{ij}\right) \Big/ \left(y_j^+ - y_j^-\right), j = 1, 2, \ldots, n \tag{15}$$

After normalization, weight assumptions need to be made for the indicators. In this paper, a balanced weight vector is set as $h = [0.25,0.25,0.25,0.25]^T$, which means the influence of each indicator is considered equally. The weighted normalized decision matrix is then expressed as:

$$G = \left(g_{ij}\right)_{m\times n} = \begin{pmatrix} h_1e_{11} & h_2e_{12} & \ldots & h_ne_{1n} \\ h_1e_{21} & h_2e_{22} & \ldots & h_ne_{2n} \\ \vdots & \vdots & \vdots & \vdots \\ h_1e_{m1} & h_2e_{m1} & \ldots & h_ne_{mn} \end{pmatrix} \tag{16}$$

where g_{ij} refers to the weighted normalized value of the *j*-th indicator under the *i*-th working condition, h_j means the weight of the *j*-th indicator.

Then, the maximum or minimum value of each indicator is obtained:

$$g_j^+ = \max_{i=1,2,\ldots,m}\left(g_{i1}, g_{i2}, \ldots, g_{ij}\right), j = 1, 2, \ldots, n \tag{17}$$

$$g_j^- = \min_{i=1,2,\ldots,m}\left(g_{i1}, g_{i2}, \ldots, g_{ij}\right), j = 1, 2, \ldots, n \tag{18}$$

For each element in the weighted normalized decision matrix, the distance calculation between the corresponding maximum or minimum value mentioned above is conducted for each indicator and then the obtained distance values will be mathematically manipulated for each indicator as follows:

$$d_i^+ = \left(\sum_{j=1}^{n}\left(g_{ij} - g_j^+\right)^2\right)^{\frac{1}{2}}, i = 1, 2, \ldots, m \tag{19}$$

$$d_i^- = \left(\sum_{j=1}^{n}\left(g_{ij} - g_j^-\right)^2\right)^{\frac{1}{2}}, i = 1, 2, \ldots, m \tag{20}$$

In order to identify the element on the Pareto frontier that is nearest to the ideal optimal solution as well as farthest from the ideal worst solution, a reference value called the relative closeness coefficient (*CC*) is introduced, as represented in Eq. (19). Obviously, the element with a smaller *CC* value is the more satisfying solution on the Pareto frontier:

$$CC_i = d_i^+ / \left(d_i^+ + d_i^-\right) \tag{21}$$

As detailed in Fig. 3, the whole optimization procedure consists of dual layers. In the first layer, the working condition optimization for each working fluid is conducted. In other words, in the first layer, for each working fluid candidate, the Pareto frontier of a population of 150 individuals is obtained after 50 generations. And the optimal working condition for each working fluid is then obtained by utilizing the TOPSIS

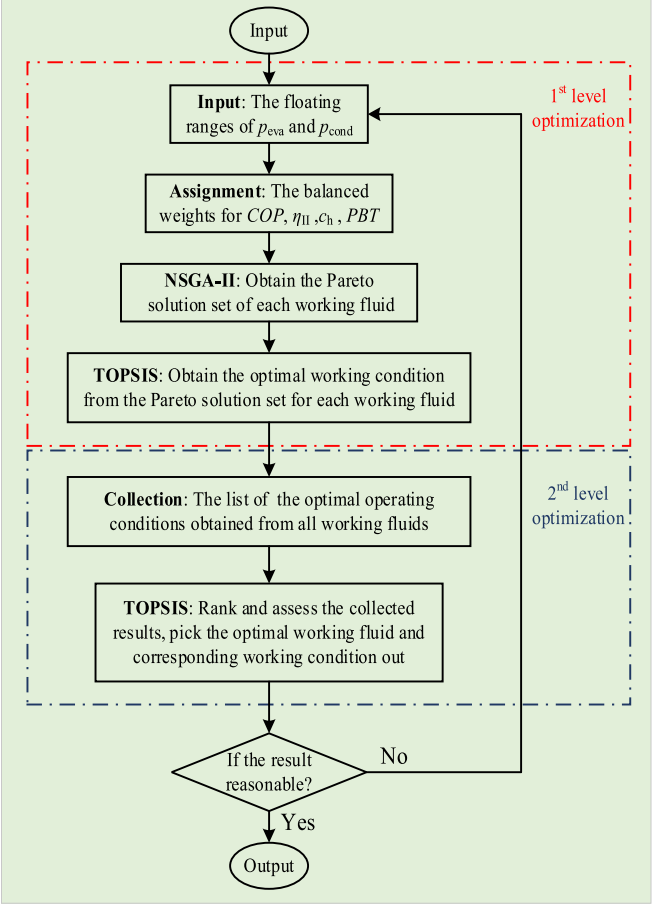

Fig. 3. The dual-layer optimization strategy framework.

method and sorting these individuals on the Pareto frontier. In the second layer, the sorting process is further carried out among the 11 working fluid candidates. The optimal values of the performance indicators under 11 working fluid candidates are collected together and the TOPSIS method is adopted again. And a list of the potential working fluid candidates with the corresponding working conditions is obtained for further analysis.

2.3. Design model of plate heat exchangers

Following the screened optimal fluid candidate and the corresponding design working condition in the dual-layer optimization process, the dimension design of the heat exchangers under different two-phase correlations then can be carried out. As mentioned above, 8 correlations would be assigned respectively to predict the two-phase heat transfer coefficients in the design processes of PHEs. A comprehensive comparison among six boiling heat transfer correlations and six condensation heat transfer correlations for heat transfer coefficient and pressure drop calculations during two-phase flow in different PHE geometries is presented in Ref. [28]. Various factors, such as experimental conditions, fluid properties, and geometries, affect the predictive accuracy of correlations. In heat pump systems, this mainly impacts performance evaluation by limiting the accuracy of heat transfer and pressure drop calculations in heat exchangers. For simplification, heat exchanger pressure drops are neglected to reduce computational demand in system simulations [64]. Similarly, this study also simplifies the model by ignoring pressure drops, following the approach in Ref. [65]. In this section, detailed design dimension parameters of the PHEs are introduced initially, followed by an explanation of the employed correlations and the subsequent design procedure for the heat exchangers.

2.3.1. Description of dimension parameters

With the regularly arranged grooves on the surface, the metal plate forms the elementary unit of PHEs. By tightly compacting multiple metal plates together, massive heat exchange channels are formed as shown in Fig. 4. Obviously, high-efficiency heat transfer can be achieved by the closely packed flow channels and sufficient heat transfer area. The morphology of plate corrugations encompasses several geometric configurations, including horizontal straight corrugations, herringbone corrugations, oblique corrugations, spherical corrugations, step corrugations, and so on. Among these, the most widely used are plates with herringbone corrugations, which are also called chevron plates [66].

The geometric structure of the plate in chevron corrugation shape is visually presented as Fig. 5. Generally, the plate design parameters can be divided into the plate size parameters and the corrugation configuration parameters. As for the plate size parameters, the plate width W of 0.5 m and thickness t of 0.0005 m are reasonably set respectively [67]. And the plate length L is the design variable of PHEs in this study, which will be calculated in the detailed mathematical solving process. The parameters that describe the plate corrugation configuration mainly include the wavelength, the and corrugation depth the chevron angle which are pre-defined in Table 4 to simplify the PHE design process. Meanwhile, considering the investment cost and thermal conductivity, stainless steel is selected as the plate material in this paper. What's more, the number of plates in the PHE is set as 200, which is a relatively large but acceptable value for the large capacity heat pump application [68].

An area-enlargement factor φ is introduced to simplify the plate area calculation considering the corrugation configuration parameters of the uneven plate. It characterizes the surface area ratio between a corrugated plate and a flat plate, which is defined as:

$$\varphi = 1 \Big/ 6 \times \left(1 + \sqrt{1 + X^2} + 4\sqrt{1 + X^2/2}\right) \tag{22}$$

where X is the dimensionless corrugation factor calculated by:

$$X = b\pi/\lambda \tag{23}$$

2.3.2. Flow boiling correlations for the two-phase region

A flow boiling correlation is often utilized for predicting the heat transfer coefficient of the two-phase region in the evaporator. For comparative analysis, 4 flowing boiling correlations (proposed by Amalfi et al. [32], Yan and Lin [33], Zhang and Haglind [34], and Liu and Winterton [29] respectively) are adopted to design the evaporator. For each flow boiling correlation, the corresponding concrete experiment conditions are summarized in Table 5 [69].

Amalfi et al. [32] collected the forecast methods for the flow boiling coefficient proposed in the past open literature and compared the predictive accuracy of each method from a large diversified database. On this basis, by dimensional and multiple regression analysis, a newly developed flow boiling correlation was fitted using a large database containing 1903 heat transfer data points. It was proved that the newly developed correlation works better than any former published one within a specific range of working conditions. The Amalfi et al. correlation is expressed as:

$$\begin{aligned} Nu_{tp} &= 982 \cdot \beta^{*1.01} We_m^{0.315} Bo^{0.32} \rho^{*-0.224}, \text{When } Bd < 4. \\ Nu_{tp} &= 18.495 \cdot \beta^{*0.248} Re_v^{0.135} Re_{lo}^{0.351} Bd^{0.235} Bo^{0.198} \rho^{*-0.223}, \text{When } Bd \geq 4. \end{aligned} \tag{24}$$

where ρ^* and Nu_{tp} represent the fluid density ratio and the Nussel number respectively.

An experimental setup was designed and employed by Yan and Lin [33] to investigate the evaporation heat transfer and pressure drop characteristics of refrigerant R134a in plate heat exchangers, revealing that the evaporation heat transfer coefficients in plate configurations significantly exceed those in circular tubes. Flow visualization was included, vividly illustrating turbulent behaviors during the evaporation

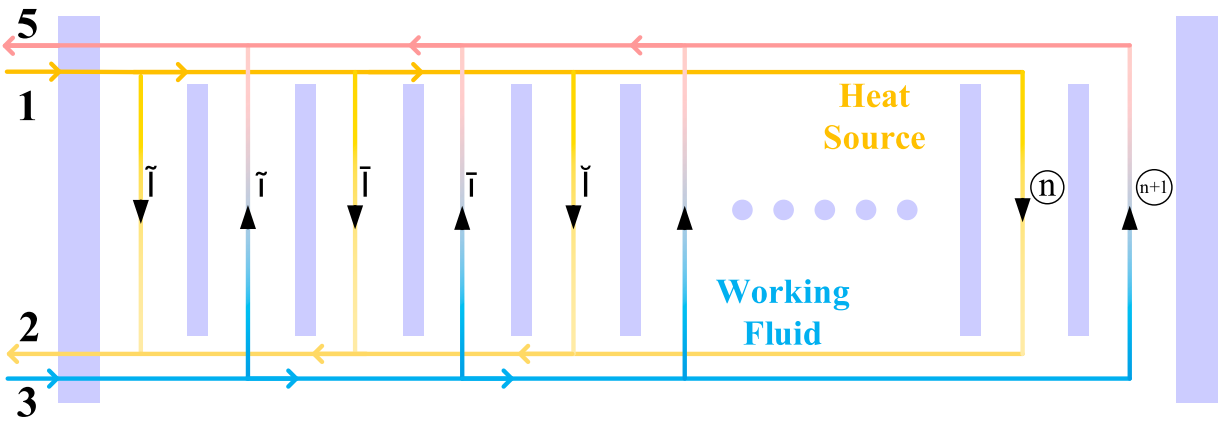

Fig. 4. Diagram of flow channels in PHEs.

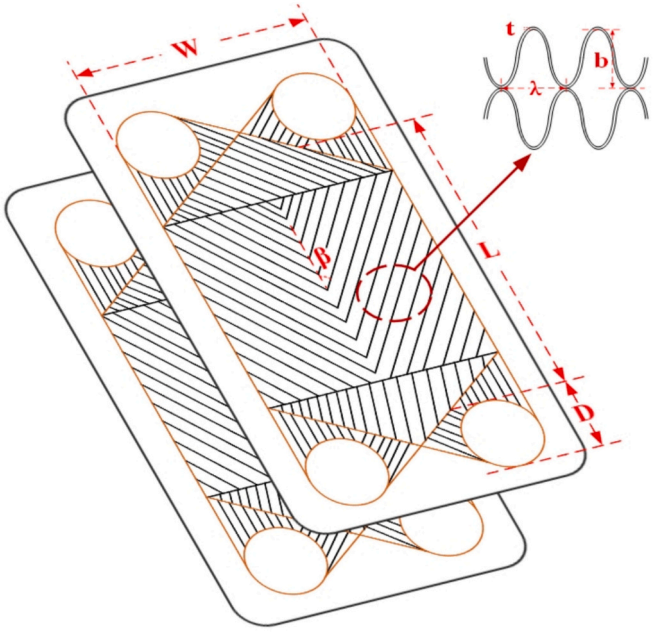

Fig. 5. The Chevron-type plate diagram.

Table 4
Assumed corrugation configuration parameters.

Parameter	Symbol	Value	Unit
Wavelength	λ	9	mm
Corrugation depth	b	2.5	mm
Area-enlargement factor	φ	1.5609	–
Chevron angle	β	60	°

process. Empirical correlations for the evaporation heat transfer coefficient and friction factor were derived by Yan and Lin [33] based on experimental data, providing practical tools for the design and optimization of heat exchangers in similar applications. Due to its concise structure and accurate prediction ability, it has been considered as a classic flow boiling correlation and has been cited by numerous literatures [70,71]. This correlation [33] is described by:

$$Nu_{tp} = d_h\alpha_{tp}\Big/k_l = 1.926Pr_l^{1/3}Bo_{eq}^{0.3}Re_{eq}^{0.5}\left[1-x_m+x_m(\rho_v/\rho_l)^{0.5}\right] \quad (25)$$

where Pr_l, Re_{eq}, Bo_{eq} and x_m refer to the liquid Prandtl number, the equivalent Reynolds number, the equivalent boiling number, and the mean vapor quality respectively.

Table 5
Experimental conditions of flow boiling tests.

Correlation	Tested fluids	G (kg/s·m^2)	T_{eva} (°C)	p_{eva} (bar)	q (kW/m^2)
Amalfi et al. [32]	R410A etc.	9 to 100	−2 to 31	–	0.14 to 41
Yan and Lin [33]	R134a	55 to 70	26 to 31	6.8 to 8	11 to 15
Zhang and Haglin [34]	R1233zd(E) etc.	52 to 137	55 to 141	14 to 28	10 to 40
Liu and Winterton [29]	Water et al.	12 to 8179	0 to 281	0.4 to 64	0.4 to 2.6

As summarized in Table 5, the experimental temperature is mainly at a low level besides the study by Zhang and Haglin. Actually, few research focuses on flow boiling processes at high-temperature levels [72]. However, the working temperature of the evaporator in the HP unit is generally at high saturation temperatures in thermal storage systems. At a relatively high temperature level (up to 141 °C), Zhang and Haglin [34] conducted the evaporation heat transfer experiment on a PHE. Due to the diversity in thermo-physical properties for different working fluids, the evaporation process was regarded as a superposition of nuclear boiling and thin-film evaporation. By linearly weighting the heat transfer coefficients predicted by Cooper et al. correlation [73] and Dittus-Boelter correlation [74], a superposition model was established for high-temperature evaporation prediction in PHEs. The results showed an excellent prediction accuracy (a mean deviation of 12.8%) and the correlation is expressed as follows:

$$\alpha_{tp} = S\alpha_{pool} + F\alpha_l \quad (26)$$

$$F = 2.35\left(X_{tt}^{-1}+0.213\right)^{0.736} \quad (27)$$

$$S = \left[1+2.53\cdot10^{-6}\left(Re_lF^{1.25}\right)^{1.17}\right]^{-1} \quad (28)$$

$$X_{tt} = (\rho_v/\rho_l)^{0.5}(\mu_l/\mu_v)^{0.1}[(1-x)/x]^{0.9} \quad (29)$$

$$\alpha_{pool} = 35P_r^{0.12}(-log_{10}P_r)^{-0.55}M^{-0.5}q^{0.67} \quad (30)$$

$$\alpha_l = 0.023Re_l^{0.8}Pr_l^{0.4}k_l/d_h \quad (31)$$

where α_{tp}, α_{pool}, and α_l denote the heat transfer coefficients of flow boiling, the pool boiling and the single-phase respectively; S means the suppression factor.

The Liu and Winterton correlation [29] has been widely adopted for

predicting the two-phase flow in tubes, which is proposed based on an abundant and diversified databank via numerous experimental data points in tubes. Considering the heat transfer process similarity, this flow boiling correlation proposed from tube experiments has also been utilized to predict the evaporation two-phase coefficient in PHEs in existing studies [49]. Therefore, this correlation is utilized as well in this paper, which is expressed as:

$$\alpha_{tp} = \sqrt{\left(S\alpha_{pool}\right)^2 + \left(F\alpha_l\right)^2} \tag{32}$$

$$\alpha_l = 0.023(k_l/d_h)Re_l^{0.8}Pr_l^{0.4} \tag{33}$$

$$\alpha_{pool} = 55P_r^{0.12}\left(-lgP_r\right)^{-0.55}M^{-0.5}q^{0.67} \tag{34}$$

$$F = \left[1 + xPr_l(\rho_l/\rho_v - 1)\right]^{0.35} \tag{35}$$

$$S = 1/\left(1 + 0.55F^{0.1}Re_l^{0.16}\right) \tag{36}$$

where α_{pool} denotes the pool boiling heat transfer coefficient.

2.3.3. Condensation correlations for the two-phase region

Four two-phase correlations (proposed by Zhang et al. [35], Kuo et al. [36], Han et al. [37], and Yan et al. [38] respectively) are adopted for designing condensers in this paper. These correlations are proposed under different experimental conditions from four various laboratories. The summary of these experiments and operating conditions is detailed in Table 6 [69].

In order to develop a condensation correlation suitable for as many working fluids or broader ranges of working conditions as possible, an in-depth investigation by Zhang et al. [35] was carried out based on several available traditional condensation correlations (including the Yan et al. [38] correlation, the Hsieh and Lin et al. correlation [75]) which are utilized commonly. In the validation and evaluation process, the correlation proposed by Zhang et al. predicted the condensation process more accurately compared with other four existing correlations (including the Yan et al. correlation [38], the Würfel and Ostrowski correlation [76], the Akers et al. correlation [77] and the Longo et al. correlation [78]). Therefore, obtained by fitting with other correlations, the validated correlation shows an excellent prediction potential for condensers. It is expressed by:

$$Nu_{tp} = 4.3375 \cdot Re_{eq}^{0.5383}Pr_l^{1/3}Bo_1^{-0.3872} \tag{37}$$

$$Bo_1 = g(\rho_l - \rho_v)D_h^2/\sigma \tag{38}$$

where Bo_1 denotes the boiling number defined in Ref. [35].

In a vertically placed PHE, Kuo et al. [36] studied the condensation process of the ozone-friendly fluid R-410A. Focusing on the influence of the operation parameters on the experimental performance, the heat transfer coefficient was less affected by the saturated pressure but directly proportional to the average vapor quality. Meanwhile, promoting effects on the condensation process were obtained as for the working fluid mass flux and imposed heat flux. A flow condensation correlation is ultimately proposed by Kuo et al. [36]:

$$\alpha_{tp} = \alpha_{r,1}\left[0.25Co^{-0.45}Fr_l^{0.25} + 75Bo_2^{0.75}\right] \tag{39}$$

$$\alpha_{r,1} = 0.2092(k_l/d_h)Re_l^{0.78}Pr_l^{1/3}(\mu_{ave}/\mu_{wall})^{0.14} \tag{40}$$

$$Fr_l = G^2/\rho_l^2 g d_h \tag{41}$$

$$Co = (\rho_v/\rho_l)[(1 - x_m)/x_m]^{0.8} \tag{42}$$

$$Bo_2 = q/Gh_{fg} \tag{43}$$

where Bo_2, $\alpha_{r,1}$, h_{fg}, Fr_l, Co, μ_{ave}, and μ_{wall} represent, as defined in Ref. [36], the boiling number, heat transfer coefficient, enthalpy drop, liquid Froude number, convection number, average dynamic viscosity and wall dynamic viscosity respectively.

With an experimental methodology similar to the laboratory of Kuo et al. [36], in the research of Han et al. [37], variation characteristics of the condensation process were explored by varying the operation parameters, based on which a condensation correlation was further proposed. It is worth noting that Han et al. [37] adopted three brazed PHEs with chevron angles of 45°, 35° and 20°. It means that the chevron angle is as well an experimental variable that is rarely mentioned in other literature. The results showed that the heat transfer coefficient increased directly with the mass flux and vapor quality, and dropped with the chevron angle or condensation temperature. This correlation is expressed as [37]:

$$Nu_{tp} = Ge_1 Re_{eq}^{Ge_2}Pr^{1/3} \tag{44}$$

$$Ge_1 = 11.22(\lambda/d_h)^{-2.83}(\pi/2 - \beta)^{-4.5} \tag{45}$$

$$Ge_2 = 0.35(\lambda/d_h)^{0.23}(\pi/2 - \beta)^{1.48} \tag{46}$$

where non-dimensional coefficients Ge_1 and Ge_2 represent the chevron-type plate geometry characteristics.

As one of the earliest classical correlations for predicting the condensation process, the Yan et al. correlation [38] has been cited by numerous literatures due to its excellent accuracy and applicability [79,80]. In the study by Yan et al., it was explored in detail the effects of working fluid status parameters on the experimentally measured heat transfer coefficients (similar conclusions were derived like those mentioned above by Kuo et al.). And the following correlation was fitted [38]:

$$Nu_{tp} = 4.118Re_{eq}^{0.4}Pr_l^{1/3} \tag{47}$$

By comparing the above experimental test conditions of the eight two-phase correlations, it can be seen that the Zhang and Haglind [34] and the Zhang et al. [35] correlations were derived based on the most similar experimental conditions with the high-temperature heat pumps. Due to the use of common test fluids (R1233zd(E) et al.), and the closest evaporation temperature and pressure ranges to high-temperature heat pumps (55 to 141 °C and 14 to 28 bar) , the Zhang and Haglind correlation [34] is considered the most suitable among the four flow boiling correlations for predicting the heat transfer performance of heat pump evaporators. Similarly, the Zhang et al. [35] correlation also adopted the familiar tested fluids (R1234ze(E) et al.) and condensation temperatures and pressures (30 to 71 °C and 2.9 to 16.3 bar), which are prevalent in the condensers of high-temperature heat pumps. Therefore, in terms of the alignment between experimental conditions and the actual operating conditions of high-temperature heat pumps, the Zhang and Haglind [34] and the Zhang et al. [35] correlations are likely the most suitable choices for the design of high-temperature heat pump evaporators and condensers, respectively.

Table 6
Operation ranges of the condensation tests.

Correlation	Tested fluid	p_{cond} (bar)	T_{cond} (°C)	q (kW/m^2)	G (kg/s·m^2)
Zhang et al.	R1234ze(E) et al.	2.9 to 16.3	30 to 71	4 to 57	16 to 90
Kuo et al.	R410A	14.4 to 19.5	–	10 to 20	50 to 150
Han et al.	R22 and R410A	–	20 to 30	4.7 to 5.3	13 to 34
Yan et al.	R134a	7 to 9	26.7	10 to 16	60 to 120

2.3.4. Correlation for the single-phase region

For the single-phase regions in evaporators or condensers, the Martin et al. correlation [81] is selected in this study. This frequently-used correlation is proposed based on the ammonia–water mixture heat transfer prediction experiment. It has been widely adopted and is defined as follows [81]:

$$Nu_{sp} = 0.122Pr^{1/3}(\mu_{ave}/\mu_{wall})^{1/6}(fRe^2 sin2\beta)^{0.374} \quad (48)$$

where f refers to the correction factor, which is given as:

$$1/f^{0.5} = cos\beta/(0.18tan\beta + 0.36sin\beta + f_0/cos\beta)^{0.5} + (1-cos\beta)/(3.8f_1)^{0.5} \quad (49)$$

when $Re < 2000, f_0 = 64/Re, f_1 = 579/Re + 3.85$,

when $Re \geq 2000, f_0 = (1.811gRe - 1.5)^{-2}, f_1 = 39/Re^{0.289}$.

2.3.5. Design workflow

Given the assumed dimension design parameters of the PHEs and based on the instruction descriptions of the utilized correlations above, the design procedure of the evaporator or the condenser is introduced in this section. Due to the theory consistency, the detailed instructions of the evaporator design process are illustrated in Fig. 6. It should be noted that, as a demonstration of the heat exchanger design process, the Yan and Lin [33] correlation is utilized for predicting the flow boiling heat transfer coefficient $\alpha_{f,x}$ of the working fluid side in the evaporator. Fig. 6 delineates an algorithmic framework employed in the iterative design methodology of the evaporator. The workflow is initiated with the specification of HP system working condition obtained in section 2.2.2 and intrinsic parameters predefined in Table 4 of this paper. A presumptive total length of the heat exchanger is posited, serving as a precursor to the sequential iterative refinement process. During each iteration, the procedure computes the thermophysical properties of the fluid within discrete control volumes, followed by the derivation of local heat transfer coefficients through different heat transfer correlations. These coefficients inform the determination of an overall heat transfer coefficient, which is instrumental in the subsequent calculation of the heat transfer area and length for each control volume. Convergence is assessed via the calculation of a length residual for each control volume, and iterative adjustments continue until the residuals fall within an

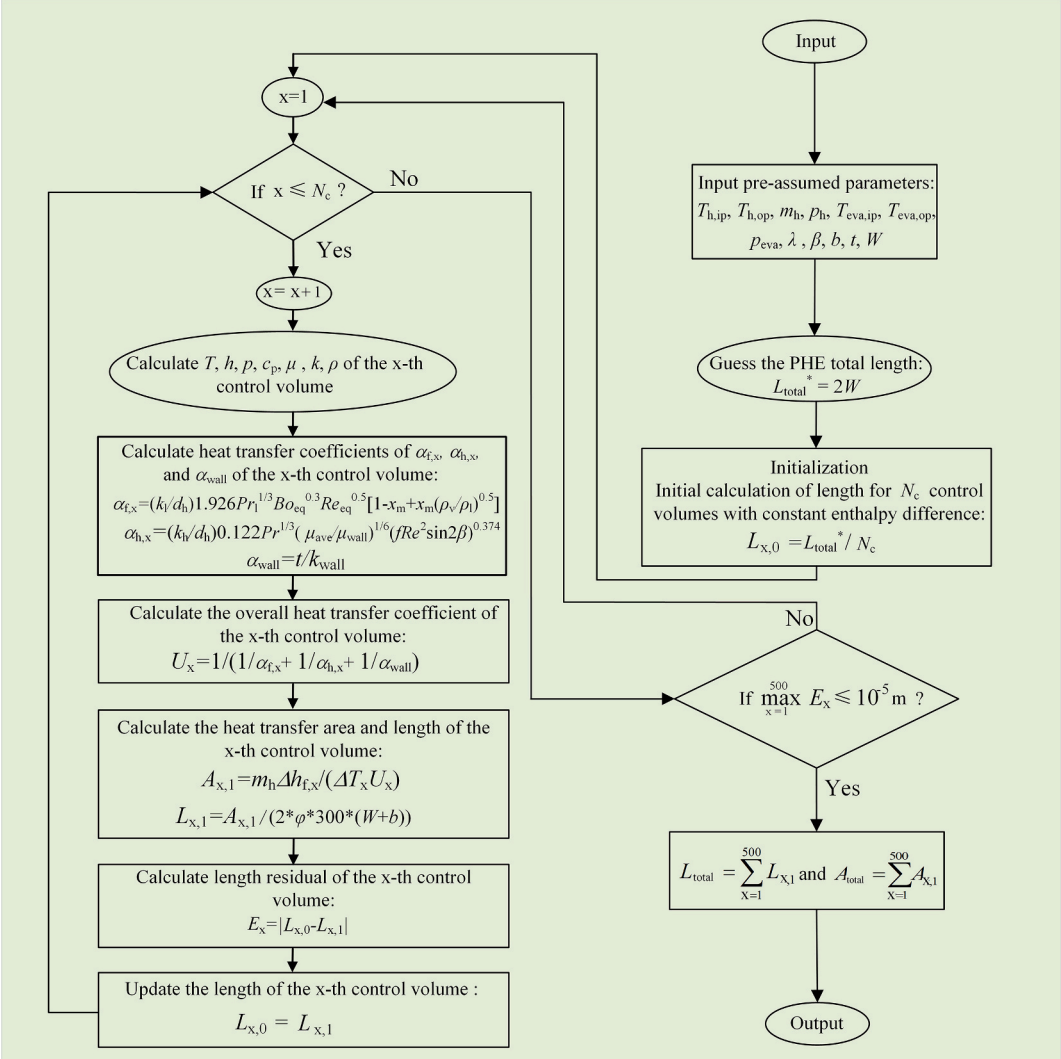

where N_c represents the number of control volumes with constant enthalpy difference and is set as 500; $\Delta h_{f,x}$ is the working fluid enthalpy drop of the x-th control volume; $\alpha_{f,x}$, $\alpha_{h,x}$, α_{Wall} are the heat transfer coefficients for working fluid, heat source and channel wall respectively; ΔT_x is the temperature difference between counter flows in the x-th control volume; $A_{x,1}$ is the updated heat exchange area of the x-th control volume; A_{total} and L_{total} are the heat exchanger total area and total length

Fig. 6. The design process of the evaporator.

acceptable margin of error (10^{-5} m). The culmination of this iterative process is the attainment of an optimized geometric configuration of the heat exchanger, characterized by the total heat transfer area and length, thus enabling the precise tailoring of the heat exchanger's performance to meet the operational exigencies.

To further illustrate in detail, adopting the finite volume method [82], the evaporator is divided into 500 micro control volumes as the basic cells for the iterative computation. As the initial input parameters, component inlet and outlet parameters are extracted from the screened optimal working condition of the HP system in the previous dual-layer optimization section. In addition, by assuming the evenly distributed enthalpy drop among the 500 control volumes, the initial plate length is calculated. In the following iteration processes of the plate length, different two-phase correlations are used to calculate the length of each control volume. The convergence criteria is set as the absolute error between the present control volume length and the previous one calculated at the last iteration step, which is set as 10^{-5} m. As long as the convergence condition is not met, the present calculated length will be inputted into the next iteration step. Repeat the above iterative calculation until the length error meets the set value, thus the size design of the evaporator is completed.

2.4. 4E evaluation model of heat pump systems

2.4.1. Transient system model nested with PHE sub-models

In the abovementioned working fluid screening procedure, the heat transfer processes of the PHEs in the HP cycle are considered by the simplified pinch point assumption, which is not sufficient for the comparative analysis among specifically utilized two-phase correlations. Hence, on the basis of the designed condensers and evaporators, the transient heat exchanger sub-models are established for rating different two-phase correlations [82]. Take the evaporator as an example, the corresponding rating program flowchart is illustrated in Fig. 7.

The flowchart in Fig. 7 delineates a computational methodology for the rating of evaporators, which is integral to the assessment of flow boiling heat transfer correlations within the transient operation of PHEs. The approach supersedes the rudimentary pinch point assumption, which is often insufficient for a detailed comparative analysis. The following points encapsulate the logistic iteration steps of the rating process:

Initialization: The procedure commences with the input of pertinent parameters of the heat source medium and the working fluid, including inlet temperatures and pressures, mass flow rates. And an assumed heat source outlet temperature is given, alongside other geometric variables of the evaporator.

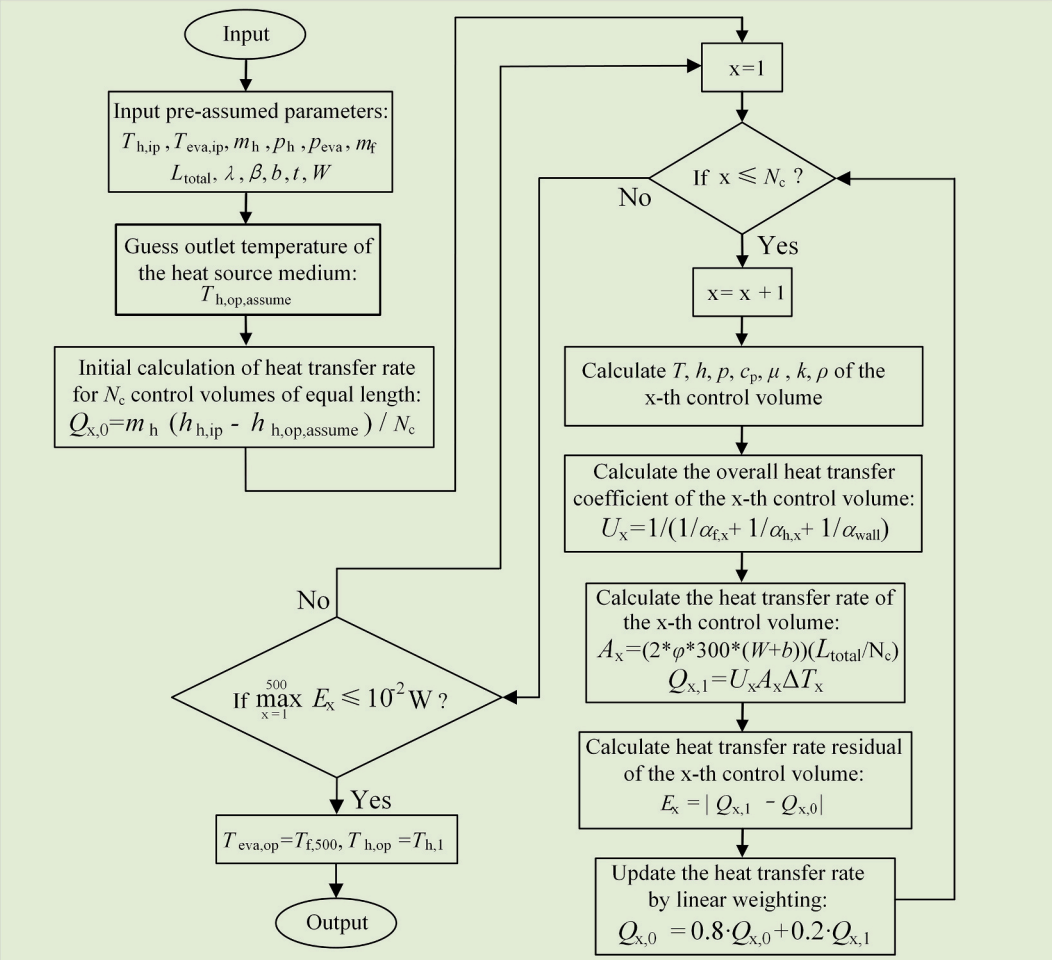

where ΔT_x is the temperature difference between counter flows in the x-th control volume; $A_{x,1}$ is the updated heat exchange area of the x-th control volume; $Q_{x,1}$ and $Q_{x,0}$ are the newly and previously calculated heat transfer rates; $T_{f,x}$, $T_{h,x}$ are the working fluid and heat source temperatures; E_x is the residual of heat transfer rate in the x-th control volume

Fig. 7. The evaporator rating procedure.

Preliminary Estimation: An initial approximation of the heat transfer rate of the x-th control volume, $Q_{x,0}$, is ascertained by dividing the initial total enthalpy change equally by the control volume designated number which is standardized at 500, with each volume being of equivalent length.

Iterative Rating: Sequentially, for each control volume:

- Thermodynamic parameters T, h, p, c_p, μ, k, ρ of the x-th control volume are computed.
- The overall heat transfer coefficient (U_x) of the x-th control volume is derived similar to the calculation procedure in Fig. 6, incorporating contributions from specific heat transfer correlations.
- These overall heat transfer coefficients are employed to calculate the heat transfer rate ($Q_{x,1}$) for each control volume, based on the mean temperature difference ΔT_x and heat transfer area A_x.

Convergence Evaluation: A residual (E_x) for the heat transfer rate is computed for each control volume. Convergence is adjudged to be achieved when the maximum residual among all the control volumes falls beneath a stipulated threshold (10^{-2} watts), indicative of the accuracy requirement being fulfilled. If the maximum residual among all the control volumes exceeds the stipulated threshold, a linear weighting coefficient group (0.8 to 0.2 ratio) would be applied to generate a new initial heat transfer rate value of the x-th control volume. The new round of iterative calculation will continue based on these given initial heat transfer rates.

Output and Validation: Upon achieving convergence, the outlet temperatures of the working fluid and heat source medium are obtained, marking the completion of the evaporator's heat transfer simulation process.

The design model (Fig. 6) predicts the plate heat exchanger's length and area for given thermal boundary conditions, while the rating model (Fig. 7) evaluates heat transfer rates under off-design conditions using the initial design parameters. These outputs are systematically compared to understand the impact of different two-phase correlation combinations on heat exchanger and system performance. The utilization of various two-phase correlations under identical inlet conditions permits the derivation of distinct outlet parameters for the heat exchangers, thereby facilitating the quantification of predictive uncertainty. Hence, this comprehensive and iterative rating process is nested into the transient system model of the HP system, which is introduced below.

To figure out how the combinations of the flow condensation and flow boiling correlations affect the system working condition prediction and performance assessment, the transient system model is established by embedding the PHE rating codes into the abovementioned fundamental system model in section 2.1. The transient system model workflow is shown in Fig. 8, which elucidates a methodical approach to embed the PHE rating codes within a foundational HP system model. This integration is pivotal to elucidating the influence of assorted flow boiling and flow condensation correlation combinations on the assessment of the system comprehensive performance. The sequential solution steps of the transient system model described within the flowchart in Fig. 8 are as follows:

Parameter Input: The model is provisioned with a set of initial input parameters which include the vapor quality at the evaporator inlet port ($x_{eva,ip}$), the condenser's inlet temperature ($T_{cond,ip}$), and the mass flow rates of the participating mediums, namely the heat source (m_h), the refrigerant (m_f), and the heat sink (m_c).

Rating Code Application: Utilizing PHE rating codes, the submodels calculate the evaporator's outlet temperature ($T_{eva,op}$) and the condenser's outlet temperature ($T_{cond,op}$), predicated on a set of predefined two-phase heat transfer correlations.

Throttle Valve Isenthalpic and Compressor Non Isentropic Calculations: The model performs an isenthalpic calculation within the throttle valve to derive the evaporator's inlet vapor quality ($x_{eva,ip}$) and an non isentropic calculation within the compressor to derive the condenser's inlet temperature ($T_{cond,ip}$), which serve as the iterative cycle's

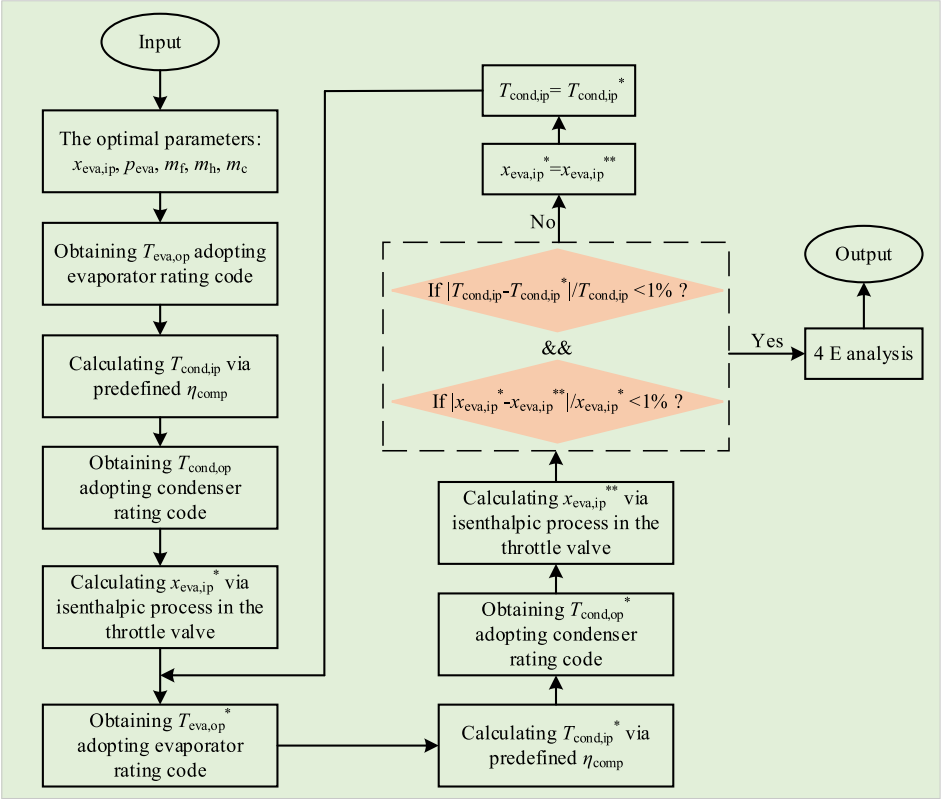

Fig. 8. The flowchart for the transient HP model.

convergence metrics.

Convergence Assessment: The system iterates until the relative error between successive calculations of $T_{cond,ip}$ and $x_{eva,ip}$ falls below a 1% threshold, indicating that a quasi-steady state has been attained.

System Performance Output: The model performs the substitution of the converging system working points into the 4E evaluation sub-model to obtain the comprehensive performance of the HP system under each specific combination of flow boiling and flow condensation correlations.

Specifically, the inlet vapor quality of the evaporator $x_{eva,ip}$ and the inlet temperature of the condenser $T_{cond,ip}$ are selected as the convergence judgment variables for the cycle convergence. The initial set parameters of the transient model include the obtained optimal inlet parameters of the evaporator with $x_{eva,ip}$ of 0.5019 and $T_{h,in}$ assumed to be either 80, 85, 90, or 95 °C, and the mass flow values of mediums (heat source $m_h = 15.9189$ kg/s, refrigerant $m_f = 20.0527$ kg/s, and heat sink $m_c = 22.1082$ kg/s). Through the iteration process, the HP cycle would gradually approach the realistic working conditions, based on which the 4E performance comparative analysis would be carried out among various two-phase correlation pairs. In addition, 4 heat source inlet temperatures $T_{h,in}$ are considered to represent both the design and off-design working conditions, varying from 80 °C to 95 °C in increments of 5 °C, which enables a comprehensive analysis of system performance under off-design scenarios. The heat source temperatures specified in this study are intentionally set at relatively high levels and, under off-design conditions, exceed the inlet temperature of the heat sink. Despite this, the outlet temperature of the heat sink consistently remains above the defined heat source temperatures, necessitating the compression of the working fluid to achieve the required temperature elevation for effective operation of the heat pump cycle. The deliberate variation in heat source temperatures serves to examine the discrepancies in heat pump performance predictions arising from different two-phase correlation combinations under off-design conditions, thereby representing a key boundary condition scenario for the comparative analysis. It is important to note that the selection of relatively higher heat source temperatures in this study was made deliberately to underscore the heat pump's performance under elevated thermal conditions, which serves as a basis for examining the system's behavior in higher-temperature scenarios. This decision aligns with the specific aim of providing a detailed case study on the operational optimization of heat pumps under off-design conditions at higher heat source temperatures.

2.4.2. Energetic assessment index

For the economic assessment, the energetic performance is quantified by the heating capacity Q_{cond} and the *COP* value. The Q_{cond} has been defined in Eq. (5), and the *COP* is defined as follows:

$$COP = Q_{cond}/W_{comp} \tag{50}$$

where W_{comp} denotes the compressor's electrical power.

2.4.3. Exergetic assessment index

Exergy is a status parameter quantifying the potential available energy, which can be expressed as following at the state point k (ex_k):

$$ex_k = (h_k - h_0) - T_0(s_k - s_0) \tag{51}$$

where the subscript 0 refers to the ambient environment.

Exergy destruction is unavoidable and is formed due to the factors such as the heat transfer temperature differences, flow friction or throttling processes. Based on the second law of thermodynamics, the exergy destruction of each component is defined as [83]:

$$Ex_{des,comp} = m_f(ex_6 - ex_5) - w_{comp} \tag{52}$$

$$Ex_{des,eva} = m_h(ex_1 - ex_2) - m_f(ex_5 - ex_3) \tag{53}$$

$$Ex_{des,cond} = m_f(ex_6 - ex_8) - m_c(ex_{10} - ex_9) \tag{54}$$

$$Ex_{des,tv} = m_f(ex_8 - ex_3) \tag{55}$$

From the principle of exergy balance, the system exergy efficiency η_{II} can be illustrated as [84]:

$$\eta_{II} = \left(1 - Ex_{des,total}/Ex_{total}\right) \times 100\% \tag{56}$$

where $Ex_{dea,toal}$ and Ex_{total} are defined as follows [83]:

$$Ex_{des,total} = Ex_{des,comp} + Ex_{des,eva} + Ex_{des,cond} + Ex_{des,tv} \tag{57}$$

$$Ex_{total} = w_{comp} + m_h(ex_1 - ex_2) \tag{58}$$

2.4.4. Economic assessment index

For the economic assessment, the c_h (levelized specific cost of heat) and *PBT* (payback time) are selected as the economic indicators. For the purpose of cost analysis, the *TCI* (total capital investment) mainly includes the following parts: the purchased equipment, assembly, installation, start-up, and other related expenses. Considering the complexity of calculating the *TCI*, a simplified definition is utilized as follows:

$$TCI = f_{TCI} \times PEC_{total} \tag{59}$$

where f_{TCI} is a factor to account for all the expenses and is assumed to be 4 [54]; PEC_{total} represents the main purchased equipment cost consisting of the expenses of the compressor and the heat exchangers, detailed expressions are listed in Table 7.

Besides the one-time investments, the annual cash flows covering the incomes and expenses are considered from 5 aspects: the income from

Table 7
Economic parameters and the corresponding formulas.

Parameter	Description	Formula	Ref.
[a]PEC_{eva}	Cost of the evaporator,	$PEC_{eva} = 15526 \times (A_{eva}/42)^{0.8}$	
PEC_{cond}	Cost of the condenser	$PEC_{cond} = 15526 \times (A_{cond}/42)^{0.8}$	[85]
PEC_{comp}	Cost of the compressor	$PEC_{comp} = 19850 \times \left(V_{comp}/279.8 \cdot \eta_{v,comp}\right)^{0.73}$	
PEC_{total}	Cost of the main components	$PEC_{total} = PEC_{eva} + PEC_{cond} + PEC_{comp}$	
TCI	Total capital investment cost	$TCI = f_{TCI} \times PEC_{total}$	
CRF	Capital recovery factor	$CRF = i_{eff}(1+i_{eff})^{n_{lt}}/\left((1+i_{eff})^{n_{lt}} - 1\right)$	
[b]CF_{TCI}	Cash flow of the total capital investment	$CF_{TCI} = CRF \times TCI$	
CF_{OM}	Cash flow of the [c]OM (Operation and Maintenance)	$CF_{OM} = f_{OM} \times TCI \times CRF$	[54]
CF_h	Cash flow of the heat source energy consumption	$CF_h = Q_{eva} \times TCI \times CRF$	
CF_{el}	Cash flow of the electricity consumption	$CF_{el} = W_{comp} \times c_{el} \times opt_{ave}$	
CF_c	Cash flow of the heat supply	$CF_c = Q_{cond} \times \eta_c \times opt_{ave} \times c_c$	
c_h	Levelized specific cost of heat	$c_h = (CF_{TCI} + CF_{OM} + CF_h + CF_{el})/Q_{cond} \cdot opt_{ave}$	
PBT	Payback time	$PBT = TCI/(CF_c - CF_{el} - CF_h)$	

[a] Purchased equipment cost.
[b] Annual cash flow.
[c] Operation and Maintenance cost, which is defined as 50 % of the total capital investment [86].

the heat supply and the expenses from the total capital investment, the operation and maintenance, the heat source energy consumption, and the electricity consumption, which are detailed in Table 7. Given the abovementioned expenses, the levelized specific cost of heat c_h and payback time *PBT* then can be calculated and obtained respectively for economic analysis.

where V_{comp} and $\eta_{v,comp}$ represent the compressor's suction volume flow rate and volumetric efficiency respectively. The electricity price is assumed to be 0.1 €/kWh and the effective interest rate is set as 5%. And the opt_{ave} denotes the annual average operation time of the heat pump system, which is defined as 8000 h per year.

2.4.5. Environmental assessment index

For environmental performance analysis, the LCCP method is utilized to quantify the carbon dioxide emission amount of an HP system. As expressed in Eq. (60), the total emission of the system during its whole lifetime can be divided into two parts. The direct part Em_{direct} is associated with the leakage and atmospheric degradation of the utilized refrigerant, which is defined as Eq. (61).

$$Em_{total} = Em_{direct} + Em_{indirect} \tag{60}$$

$$Em_{direct} = C \times (L_{ea} \times ALR + EOL) \times (GWP + Adp.GWP) \tag{61}$$

where C stands for the mass of the refrigerant charge; L_{ea} represents the average lifetime of the equipment. ALR denotes the annual proportion of refrigerant leakage, and EOL signifies the refrigerant leakage ratio at the end of life. GWP is the abbreviation for Global Warming Potential value, which measures the impact of the refrigerants on global warming. Lastly, Adp.GWP refers to the Global Warming Potential value of the Atmospheric Degradation Product, indicating the secondary effects of the refrigerant breakdown in the atmosphere.

Due to the limited reference data from the available literature, it is necessary to emphasize the refrigerant properties of R1234ze(Z), such as the GWP, Adp.GWP and so on, are supposed the same as the existing fluids R1234yf and R1234ze(E) for the purpose of comparative analysis. And detailed assumed values are illustrated in Table 8.

where EM, MM, *mr*, RM, RFM and RFD represent the CO_2 emission per kWh electricity consumption, CO_2 emission per kg manufactured material, recycled material mass, CO_2 emission per kg recycled material, CO_2 emission per kg manufactured refrigerant and CO_2 emission per kg recycled refrigerant respectively.

The indirect part $Em_{indirect}$ is associated with the energy consumption, manufacturing of the material and refrigerant, and recycling of the material and refrigerant, which is defined as [87]:

$$Em_{indirect} = L_{ea} \times AEC \times EM + \sum (m \times MM) + \sum (mr \times RM) + C \times (1 + L_{ea} \times ALR) \times RFM + C \times (1 - EOL) \times RFD \tag{62}$$

where *AEC* and *m* represent the annual electricity consumption and total equipment mass respectively. The detailed assumptions are illustrated in Table 8. What's more, the *AEC*, m_{comp}, m_{eva}, m_{cond} and m_{tv} are calculated by the following equations:

$$AEC = opt_{ave} \cdot W_{comp} \tag{63}$$

$$m_{comp} = 31.22 \cdot W_{comp} \tag{64}$$

$$m_{eva} = \rho_{steel} \times t \times A_{eva} \tag{65}$$

$$m_{cond} = \rho_{steel} \times t \times A_{cond} \tag{66}$$

$$m_{tv} = 0.2 \cdot m_{cond} \tag{67}$$

where opt_{ave} is the system annual operation time assumed as 8000 h, and t is the plate thickness of PHEs.

It is worth pointing out that the economic evaluation model and LCCP environmental assessment method used in this study were chosen due to their simplicity and speed of calculation. However, for more accurate economic and environmental performance evaluations, it is necessary to consider factors like carbon pricing or lifecycle costs. Overall, the simplified model used in this study has not lost the representational significance of the indicators themselves. To investigate the influence of different two-phase correlations on the plate heat exchanger design and HP system off-design performance, this study is arranged and consists of three sequential steps. In the first step, based on the consistent and unified preconditions defined in Table 2, Table 4, and Table 8, 11 types of refrigerants are screened to obtain a suitable working fluid along with the system design working condition which is utilized as the consistent and unified boundary condition for the evaporator and condenser designs under various two-phase correlations. In the second step, regarding the obtained working condition as design condition, the influence of various correlations on the heat exchangers is discussed from the dimensional, economic and environmental aspects. In the third step, the effects of 16 pairs of correlation combinations on system performance are examined to elucidate the relationships between different correlations and variations in heat pump performance indicators. The exergy destruction rates of components and the exergy efficiencies of the system are presented for comparative analysis. Among the various correlation pairs, the levelized specific cost of heat (c_h) and the payback time (*PBT*) are compared in the economic analysis, and the Life Cycle Climate Performance (LCCP) assessment method is employed in the environmental analysis. The simulations were performed using MATLAB R2018a with the user-defined function for iterative calculations. And the computations were conducted on a desktop workstation with an Intel Core i9 12900K processor and 64 GB RAM.

3. Results and discussion

3.1. Screening results of the system thermo-economic optimization

Based on the abovementioned dual-layer optimization strategy, the optimized working conditions of the 11 working fluid candidates are obtained by the NSGA-II algorithm under the balanced weights of 4

Table 8
The assumed values of parameters to calculate the emissions.

Parameter	Value
C	2.7 kg/kW$_{hc}$ [87]
mr	0.07 kg
L_{ea}	20 years
ALR	5%
EOL	15%
GWP of R1234ze(Z)	6 (for comparative analysis) [88]
Adp.GWP of R1234ze(Z)	3.3 (for comparative analysis) [89]
EM (Steel)	1 kg CO_{2e}/kwh
MM (Steel)	2.46 kg CO_{2e}/kg
RM (Steel)	0.07 kg CO_{2e}/kg
RFM of R1234ze(Z)	13.7 kg CO_{2e}/kg (for comparative analysis) [63]
RFD of R1234ze(Z)	1.16 kg CO_{2e}/kg (for comparative analysis) [63]

Table 9
Optimized thermo-economic performance of fluid candidates.

Candidate	p_{eva} (bar)	p_{cond} (bar)	*COP* (−)	η_{II} (%)	c_h (€/MWh)	*PBT* (years)
R1234ze(Z)	3.799	17.653	3.524	51.986	40.217	2.689
R600	4.892	19.027	3.468	51.420	40.676	2.793
R600a	6.775	23.816	3.238	49.056	42.323	3.080
R114	4.434	17.927	3.236	49.040	43.130	3.625
R1224yd(Z)	3.276	16.685	3.107	47.666	44.081	3.849
R124	7.717	28.620	3.073	47.307	43.548	3.305
R236ea	4.526	20.426	3.069	47.257	44.395	3.944
R245fa	3.413	19.429	2.928	45.711	45.639	4.396
R236fa	5.801	24.206	2.836	44.678	46.604	4.894
R1234ze(E)	8.672	32.626	2.783	44.078	47.099	5.163
R1233zd(E)	2.928	18.167	2.783	44.077	47.549	5.651

objective functions. As listed in Table 9, through the TOPSIS method, the fluid candidates then are ranked according to their thermo-economic behaviors. To present a more intuitive comparison among competitive potential fluids, the optimized objective function values (*COP*, η_{II}, c_h, *PBT*) of the top 5 candidates in Table 9 are displayed as Fig. 9. Obviously, the fluid candidate R1234ze(Z) achieves an excellent thermodynamic performance with the maximum *COP* and η_{II}, and the minimum c_h or *PBT* is also obtained by R1234ze(Z). The other 4 candidates show a more inferior performance in the thermodynamic or economic aspect, especially for the refrigerant R1224yd(Z). Taking the environmental protection properties of the refrigerants into consideration, the other 3 traditional working fluids R600, R600a and R114 possesses a relatively high GWP value (>3). R600 and R600a are flammable refrigerants with the SG index of A3. Therefore, the low-GWP (GWP < 1) refrigerant R1234ze(Z) is preferred in this paper due to its benefit in improving the environmental performance of heat pumps. In addition, the working pressure of R1234ze(Z) is the second lowest among the top 5 candidates, which means a safer and more reliable working condition for the heat pump components. Hence, through consideration of thermo-economical performance, equipment safety and environmental protection, R1234ze (Z) is picked out as the optimal fluid and the corresponding optimal working condition is operated under the p_{eva} of 3.799 bar and the p_{cond} of 17.653 bar.

3.2. Design results of heat exchangers

On the basis of the screened refrigerant R1234ze(Z), the corresponding HP cycle working condition is further set as the design condition of the condensers and evaporators. By varying the flow condensation correlations or flow boiling correlations, the designed dimension results including the plate length and total heat transfer surface area are shown in Fig. 10 and Fig. 11 respectively. Due to the distinct differences in the mathematical expressions or prediction behaviors among different correlations, apparent variation of the design results is observed. For the condenser, the maximum plate length is estimated via the Zhang et al. correlation [35], which reaches nearly 2.36 times the minimum value calculated through the Kuo et al. correlation [36]. For the evaporator, the maximum plate length value assessed via the Zhang and Haglind correlation [34] is 2.06 times the minimum value calculated by the Amalfi et al. correlation [32]. Similar results about the total heat exchange area are obtained as the length and area of a plate are directly proportional to each other under the given plate structure pre-definition in this paper. It is clear that the influence of different correlations is significant and cannot be neglected in the heat exchanger dimension design process.

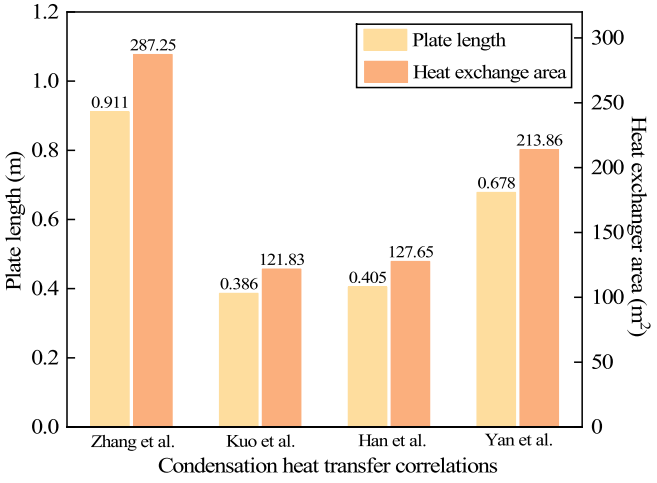

Fig. 10. Design results of condensers.

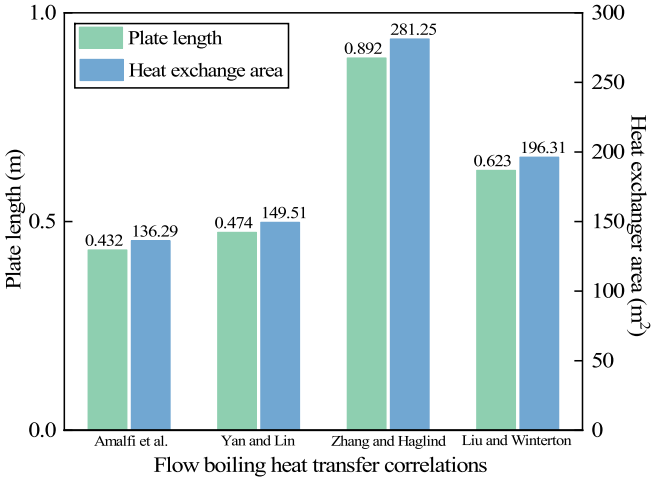

Fig. 11. Design results of evaporators.

Furthermore, the purchasing cost and manufacturing carbon emission of the heat exchangers are compared among various correlations. When considering the carbon emission of heat exchangers, only the

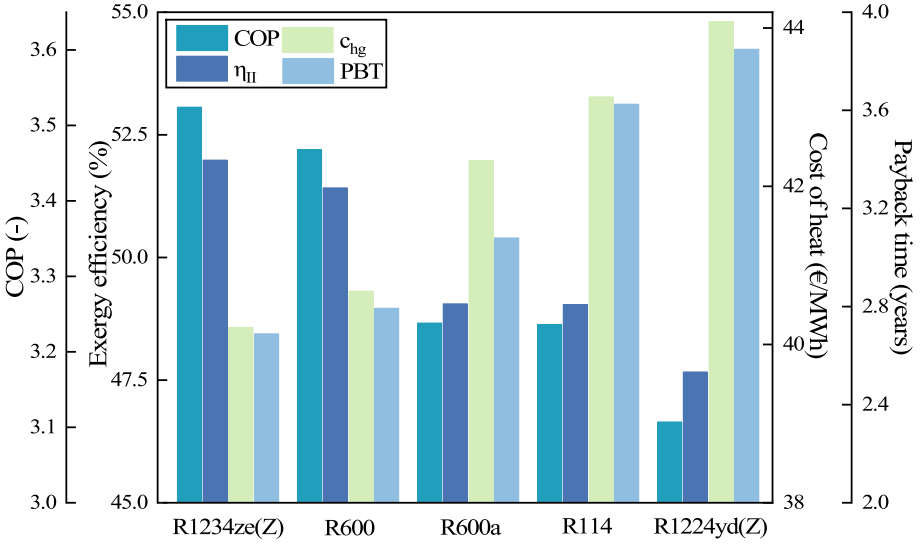

Fig. 9. Top five optimal candidates by TOPSIS sorting.

manufacturing process is involved as the carbon emission amount of the recycling process can be nearly ignored [90]. As shown in Fig. 12, a relative difference in the condenser costs (98.6%) is gained between the highest cost calculated by the Zhang et al. correlation [35] and the lowest cost evaluated by the Kuo et al. correlation [36]. And a relative difference in the evaporator costs (78.5%) is also obtained between the maximum cost calculated by the Zhang and Haglind correlation [34] and the minimum cost evaluated via the Amalfi et al. correlation [32]. From economic assessment aspects, the selection of two-phase correlations has an apparent effect on both the condenser and the evaporator. As displayed in Fig. 13, the distribution pattern of the heat exchanger carbon emissions is highly consistent with the heat exchanger costs. It can be explained that the calculation of carbon emissions for heat exchangers solely considers the direct emissions resulting from the material usage in manufacturing. As indicated by Eq. 60, Eq. 63, and Eq. 64, the carbon emissions are directly proportional to the mass of the heat exchanger, which in turn is directly proportional to the heat exchanger area. This implies that the carbon emissions are directly proportional to the area of the heat exchanger. And as shown in Table 6, the cost calculation for heat exchangers also demonstrates that the cost is positively correlated solely with the heat exchanger area. Therefore, both emissions and costs are primarily influenced by the area of the heat exchanger. Likewise, the maximum relative differences of the condenser and evaporator carbon emissions 134.7% and 106.1% are obtained respectively.

During the design procedure of heat pump heat exchangers, 8 two-phase correlations were selected and replaced (4 of flow condensation ones and 4 of flow boiling ones) to investigate their impact on the theoretical dimensions, cost and carbon emissions of the heat exchangers designed. An apparent distinction of the dimensions and performance indexes was obtained among the designed condensers or evaporators, such as an uncertainty of 134.7% for the condenser carbon emission and an uncertainty of 106.5% for the evaporator dimension. Therefore, from the viewpoint of components, choosing and utilizing various two-phase correlations affects the heat exchanger's dimension design and performance assessment significantly, which could lead to a remarkable deviation in the whole heat pump system performance evaluation.

3.3. Comparative analysis under different correlations

3.3.1. Energetic and exergetic comparative analysis

It is unforeseeable that whether the differences in heat exchanger performance predictions would lead to different heat pump system

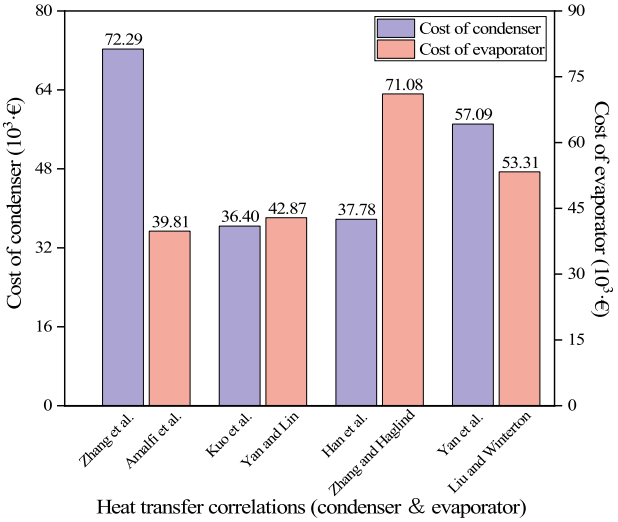

Fig. 12. Cost of heat exchangers.

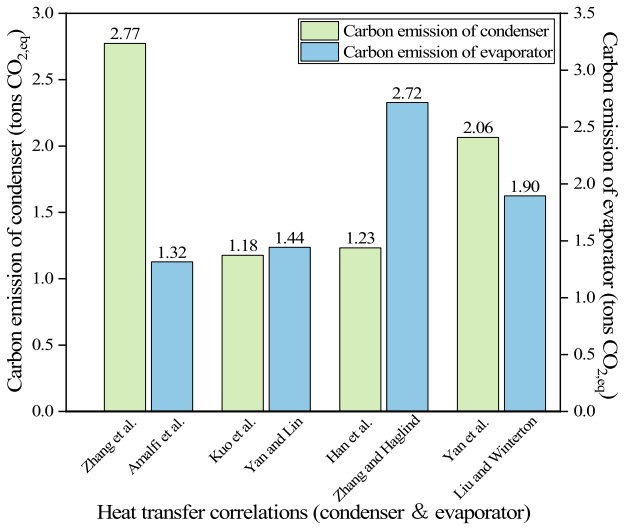

Fig. 13. Carbon emission of heat exchangers.

performance assessment results under different pairs of two-phase correlation combinations. Thus, to investigate this potential influence of two-phase correlation selections on the whole system, 16 sorts of two-phase correlation combinations are compared and discussed, which are represented by the substitution symbols given in Table 10. According to the 4E analysis method [50], the energy and exergy aspects are firstly explored in this section. As mentioned above, the heat exchangers were designed when T_h was fixed at 80 °C, based on which another three levels (T_h = 85, 90, 95 °C) are further considered as the complement to off-design conditions.

Energy analysis for thermodynamic cycles is conducted from the aspect of energy's amount. Comparison of the HP cycle heating capacity among various correlation pairs under 4 heat source conditions is exhibited as Fig. 14. At each specific T_h, the heating capacity fluctuates with the correlation pairs and a maximum relative difference is obtained. It's obvious that the curve fluctuation at the design condition is smaller than that at the other three heat source temperatures. This is because that all the heat exchangers are designed at T_h = 80 °C and a given heat exchange amount of the evaporator (2 MW). And in the following detailed system modeling as described in Fig. 8, only the similar boundary condition of T_h = 80 °C is constrained, which would lead to the analogous convergence results of the evaporator and also the whole system under different correlation pairs. From another point of view, a maximum relative difference of 1.45% also verifies that all the heat exchangers are designed properly from different two-phase correlations and perform similarly under the predefined design condition. Under the other 3 heat source conditions, all the minimum heating capacity values are predicted by the correlation pair C-1. While the maximum heating capacity values are predicted by the correlation pairs C-10, C-11 and C-12 at T_h = 85 °C, 90 °C and 95 °C respectively, with the relative difference values of 9.88%, 7.23% and 6.33%. Hence, the selection of the two-phase correlations has a notable influence on the system heating capacity prediction.

COP is widely recognized as the most important indicator for characterizing the cycle performance. As shown in Fig. 15, as the T_h

Table 10
Substitution symbols of two-phase correlation pairs.

Two-phase correlations	Amalfi et al. [32]	Yan and Lin [33]	Zhang and Haglind [34]	Liu and Winterton [29]
Zhang et al. [35]	C-1	C-5	C-9	C-13
Kuo et al. [36]	C-2	C-6	C-10	C-14
Han et al. [37]	C-3	C-7	C-11	C-15
Yan et al. [38]	C-4	C-8	C-12	C-16

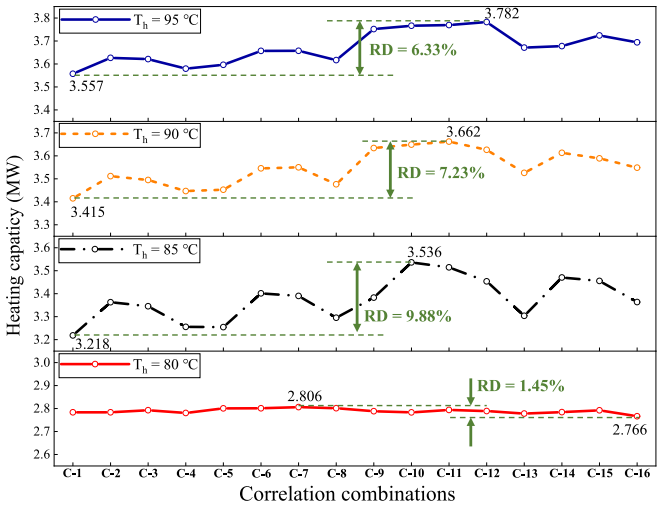

Fig. 14. Comparison of heating capacity under various T_h.

increases, the *COP* value reaches a higher level under each specific correlation pair, which is consistent with previous studies [91]. Similar to the variation characteristic of the heating capacity, the predicted *COP* values among different correlation pairs fluctuate under off-design conditions and vary most obviously at $T_h = 85$ °C with a relative difference value of 3.27%. As a dimensionless performance index, improvement of the *COP* is usually difficult for a realistic heat pump system. Hence, this floating range cannot be ignored and should be taken into consideration in the cycle performance assessment process.

Exergy analysis for thermodynamic cycles is conducted from the aspect of energy's grade. In Fig. 16, the heatmap of cycle exergy efficiency η_{II} exhibits that the difference among different correlation pairs is tiny at the design heat source condition while large at off-design conditions. At $T_h = 80$ °C, the relative difference of η_{II} is as low as 0.31% which is tiny enough to be ignored. However, the relative difference values of η_{II} at $T_h = 85$, 90 and 95 °C are 3.67%, 5.74% and 6.76% respectively. Therefore, the utilization of different correlations may cause a large uncertainty of the heat pump cycle exergy efficiency prediction under off-design conditions.

To further explore the intrinsic relationship with this difference, at $T_h = 95$ °C of the highest η_{II} uncertainty, the exergy destruction distribution of the components is illustrated in Fig. 17. The exergy destruction composition of the system is consistent with former simulation studies with a main proportion of the condenser and the throttle valve [92]. Among the 16 correlation pairs, the exergy destruction of the compressor or evaporator hardly varies while a relative apparent change of the condenser or throttle valve is perceived. As the throttle process in the expansion valve is considered to be isenthalpic, which absolutely differs from the realistic operation condition in existing experimental research [83,93]. Hence, under different heat two-phase correlation combinations, different iterative convergence results of the heat pump operating conditions lead to the differences in exergy destruction distribution among the components, with the condensing heat exchanger correlation playing a major role shown in Fig. 17. Additionally, it is worth pointing out that compared with experimental studies [94], the results predicted by simplified models of the compressor and the expansion valve may be of limited reference significance.

3.3.2. Economic and environmental comparative analysis

In order to comprehensively evaluate the heat pump system performance, economic and environmental indicators have been defined and

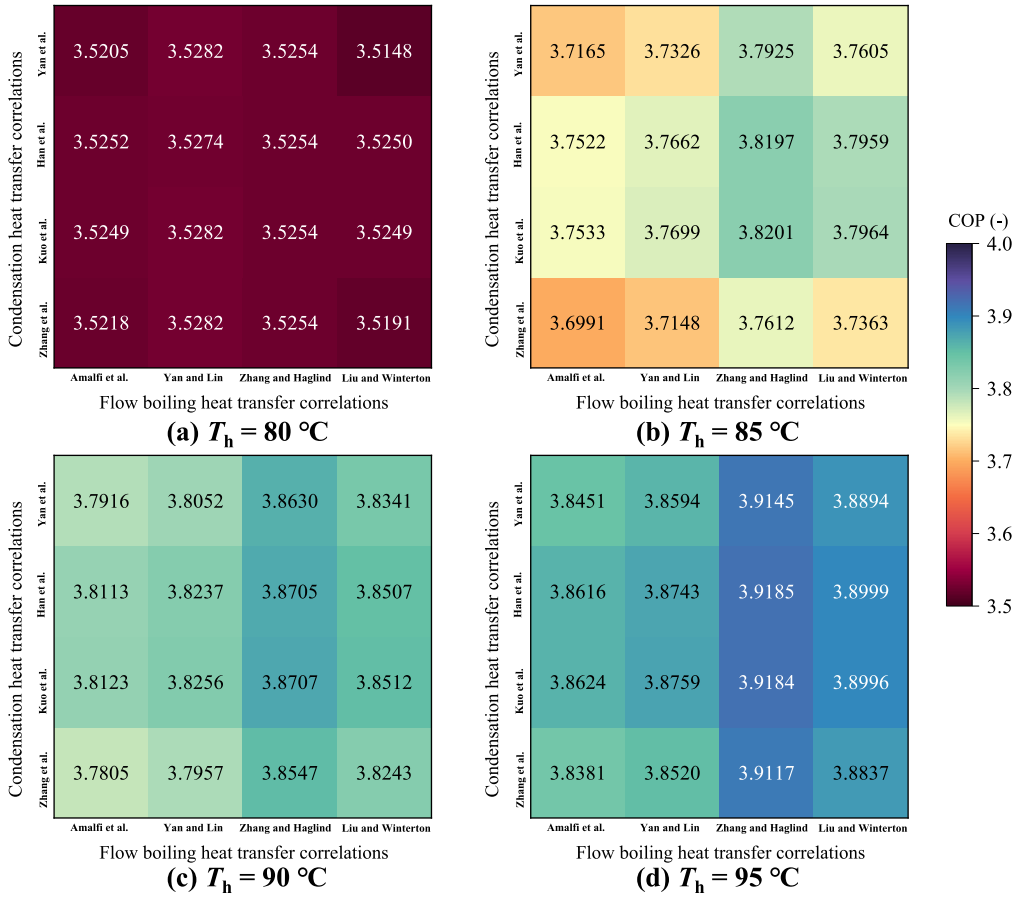

Fig. 15. Comparison of *COP* under various T_h.

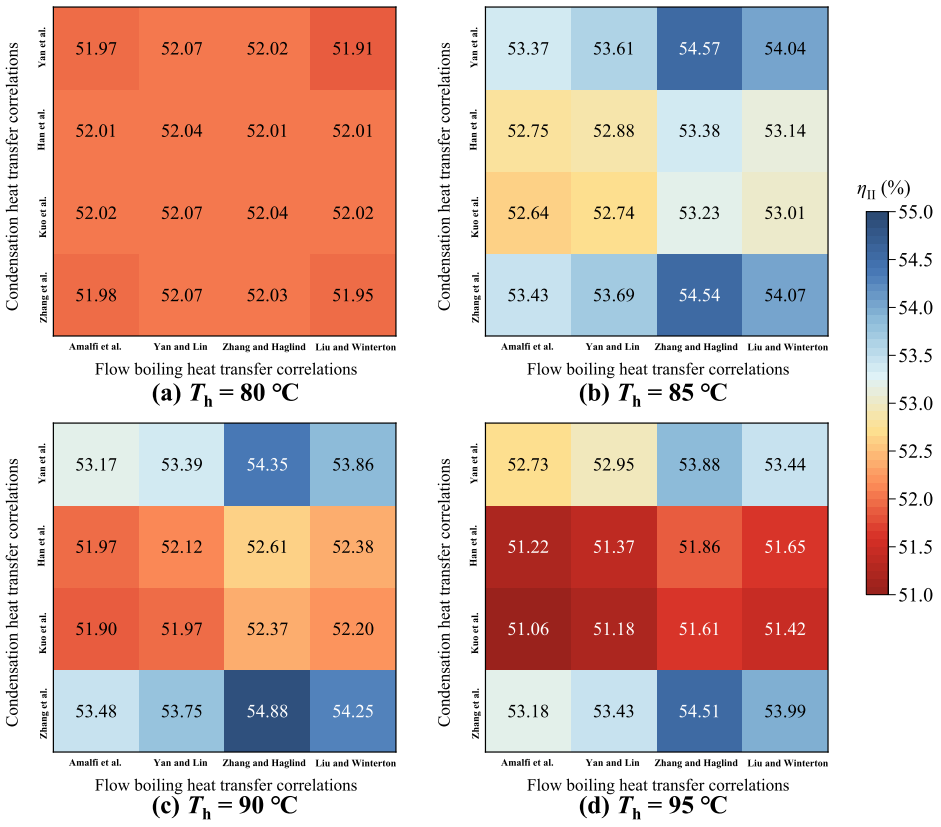

Fig. 16. Comparison of η_{II} under various T_h.

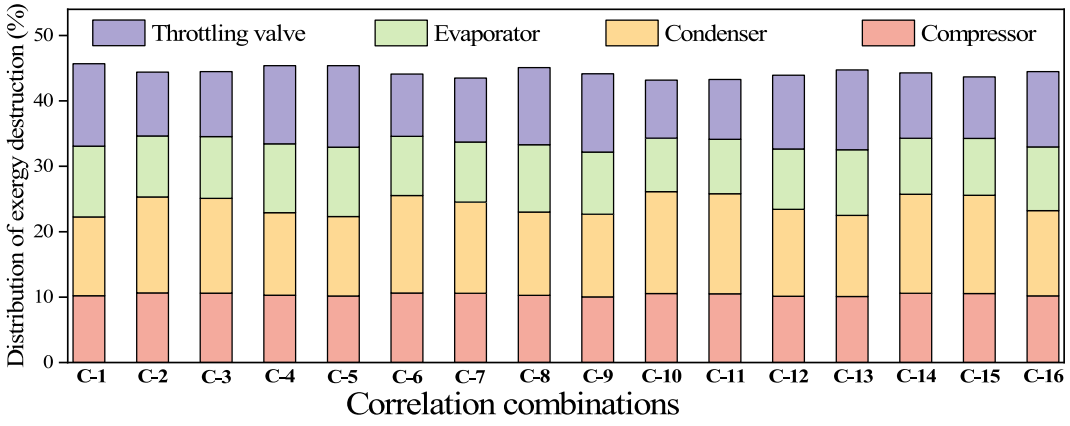

Fig. 17. Comparison of exergy destruction distribution at T_h = 95 °C.

widely utilized using common calculation models [47,95]. For the economic aspect, the main purchased equipment cost PEC_{total}, levelized specific cost of heat c_h and payback time *PBT* are discussed and compared in this study. As displayed in Fig. 18, the variation of PEC_{total} among 16 correlation combinations is obvious and the maximum relative difference of 29.65% is obtained between correlation pairs C-2 and C-9. As the heat exchangers are the main components of the heat pump system, the selection of two-phase correlations shows a significant influence on the PEC_{total}. In addition to considering the cost of main components, other aspects such as the assembly, installation, operation, loan interest rate and other related expenses are included by the levelized specific cost of heat c_h and payback time *PBT*, which therefore are often utilized in comprehensive economic analysis. As shown in Fig. 19, the very small difference of c_h (0.26%) is reflected among 16 correlation pairs at the design heat source temperature T_h = 80 °C. While at T_h = 85 °C, a slight distinction (the maximum relative difference of 1.91%) is observed. With T_h increasing to 90 and 95 °C, this distinction (the maximum relative differences of 1.22% and 1.04% respectively) is gradually disappearing. Presumably, by the definition illustrated in Table 7, it should be the case that as the temperature of the heat source rises, the numerator annual investment cost changes by a quantitatively smaller amount than the denominator annual heat capacity, and the difference in the ratio ultimately obtained is weakened as the denominator base becomes progressively larger. To sum up, the cost of heat c_h is influenced by the correlation selections in a limited extent.

As shown in Fig. 20, it can be seen that the economic performance index *PBT* gradually decreases with T_h under each correlation pair. This can be explained by the rising trend of the heating capacity displayed in Fig. 14. According to Eq. (59), the total capital investment *TCI* is a constant value under each correlation combination case, while the

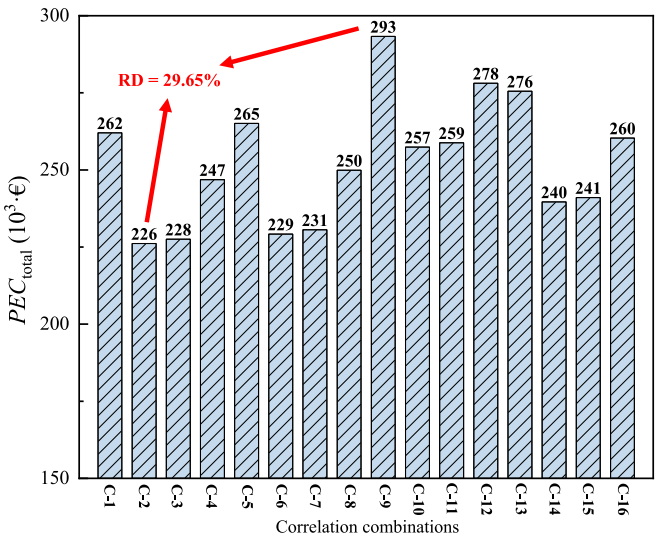

Fig. 18. Comparison of PEC_{total} under various correlation pairs.

increase in heating capacity leads to the increment of the annual cash flow, which further results in a decrease in *PBT*. Among the investigated 16 pairs of correlations, the maximum relative difference of *PBT* at T_h = 80 °C is as small as 0.89%. At the T_h = 85, 90 and 95 °C, all the values of the maximum relative differences (4.44%, 2.19% and 3.45% respectively) are within 5%, which means the *PBT* is affected by the two-phase correlation selections to a certain extend.

Finally, by the environmental analysis method LCCP, the total equivalent CO2 emissions of the heat pump systems under different heat source temperatures are exhibited in Fig. 21. Consistent with the abovementioned findings, little difference (1.08%) in system carbon emissions is predicted by different correlation combinations at T_h = 80 °C. Also, a visible distinction among the 16 pairs of correlations is perceived at T_h = 85, 90 and 95 °C with the maximum relative difference of 6.38%, 4.73% and 4.24% respectively. From the comparative analysis, it can be concluded that the choice of two-phase correlations may cause a visible uncertainty in the environment performance evaluation index.

4. Conclusions

To investigate the influence of different two-phase heat transfer correlations on the heat pump system performance assessment, a comparative study was conducted from the heat exchanger design and the system's 4 E performance. 8 two-phase correlations (4 flow boiling ones proposed by Amalfi et al. [32], Yan and Lin [33], Zhang and Haglind [34], and Liu and Winterton [29]; 4 flow condensation ones suggested by Zhang et al. [35], Kuo et al. [36], Han et al. [37], and Yan et al. [38]) were investigated and compared in this study. Obtaining the screened optimal fluid candidate R1234ze(Z) and the corresponding working condition for designing heat exchangers, in the component viewpoint, the dimension, economy and environment distinctions among designed heat exchangers were focused and compared. Further, from the system viewpoint, a comparative analysis of the heat pump

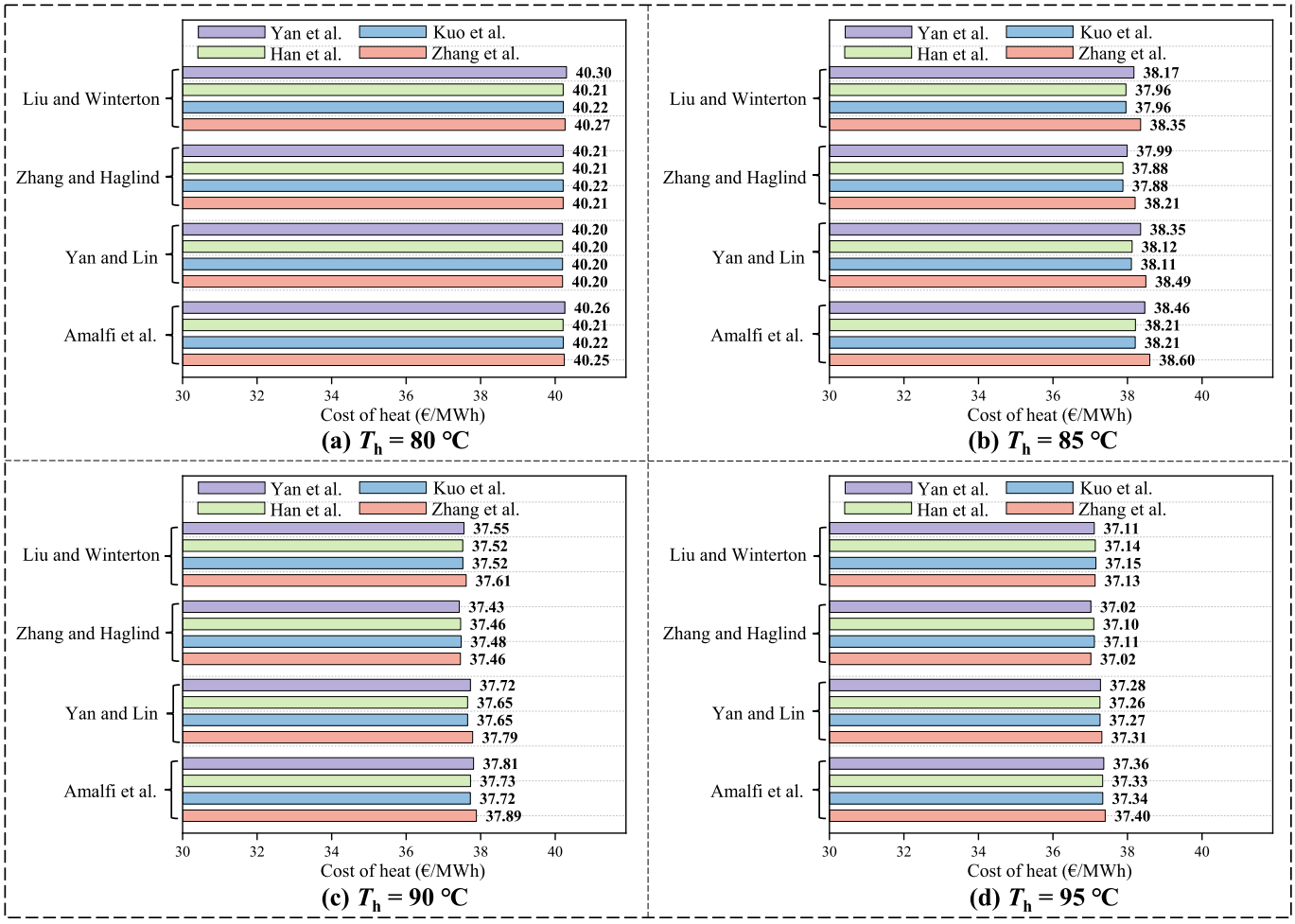

Fig. 19. Comparison of c_h under various T_h.

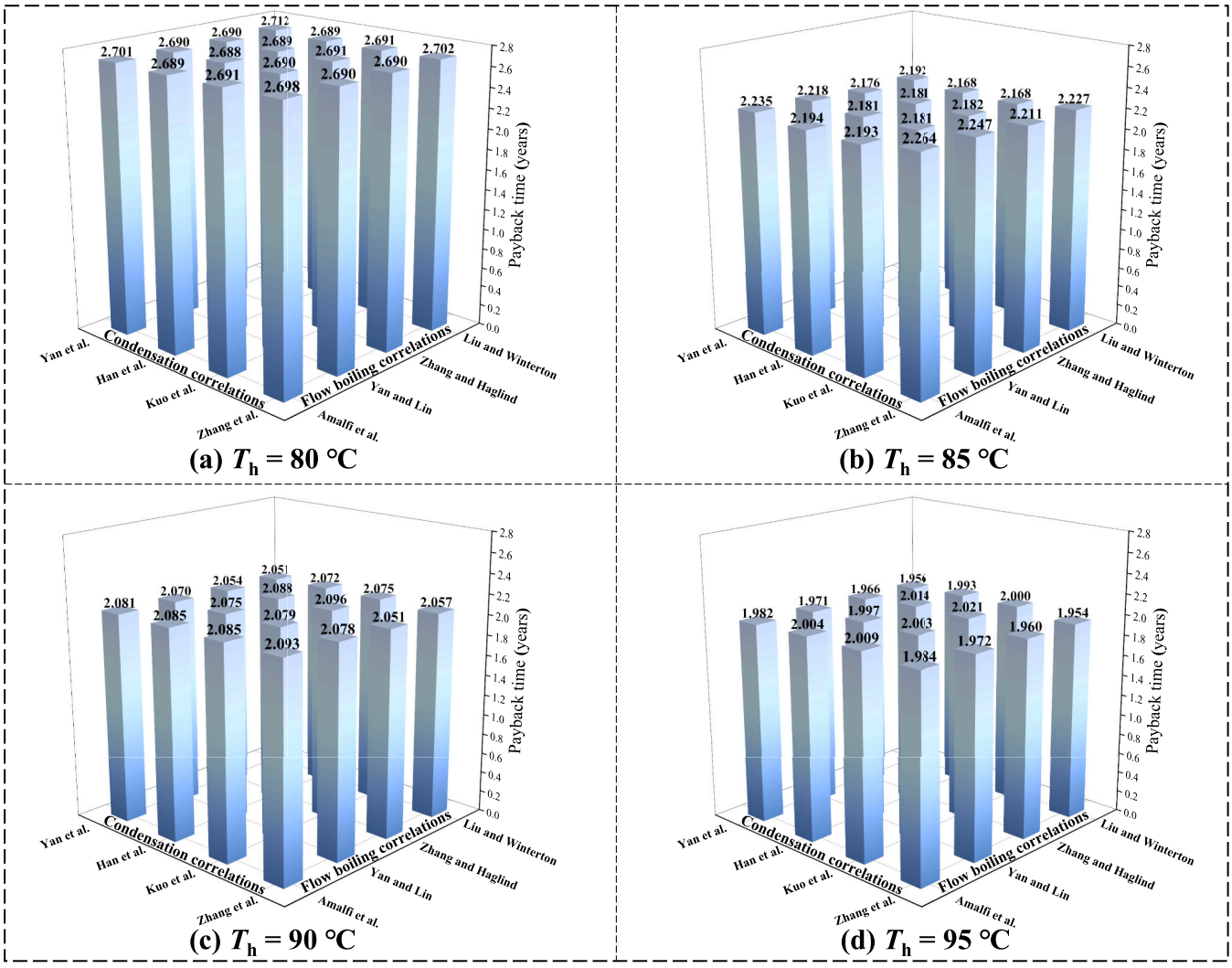

Fig. 20. Comparison of *PBT* under various T_h.

system performance assessment was conducted under the 4 E analysis method. The major conclusions are illustrated as:

1) Given that the Zhang and Haglind correlation [34] and the Zhang et al. [35] correlation were developed under experimental conditions closely resembling those in the evaporator and condenser of high-temperature heat pumps (e.g., similar working fluids and temperature ranges), these correlations appear to provide reliable predictions for plate heat exchanger design among the eight evaluated. However, further experimental validation across diverse PHE geometries and a wider range of operating conditions is essential to confirm their accuracy.

2) During the heat exchanger design procedure, the selection of the two-phase correlations had a significant impact on the theoretical dimensions, cost and carbon emissions of the condensers and evaporators. For the condenser, the obvious relative distinctions (136.0% of the dimension, 98.6% of the cost and 134.7% of the carbon emission) were found between the Zhang et al. correlation [35] and the Kuo et al. correlation [36]. And for the evaporator, a noticeable relative difference (106.5% of the dimension, 78.5% of the cost and 106.1% of the carbon emission) was found between the Zhang and Haglind correlation [34] and the Amalfi et al. correlation [32].

3) As for the systems' energy and exergy behaviors, under the design heat source temperature, little relative distinctions (1.45% of the heating capacity, 0.38% of the *COP* and 0.31% of the exergy efficiency) were observed. While under the off-design heat source temperatures, obvious relative distinctions (9.88% of the heating capacity, 3.27% of the *COP* and 6.76% of the exergy efficiency) were derived.

4) As for the systems' economy and environment behaviors, under the design heat source temperature, tiny relative differences (0.26% of the heating cost c_h, 0.89% of the payback time *PBT* and 1.08% of the carbon emission) were gained. While under the off-design heat source temperatures, much higher relative differences (1.91% of the heating cost c_h, 4.44% of the payback time *PBT* and 6.38% of the carbon emission) were obtained.

5) Among the correlations studied, the Zhang et al. correlation [35] might lead to a low level of the COP value, while the Zhang and Haglind correlation [34] produced the opposite effect. The correlation proposed by Zhang et al. [35] or Zhang and Haglind [34] predicted a much high exergy efficiency and the lower level of exergy efficiency was derived by the Kuo et al. correlation [36] or the Amalfi correlation [32]. The Zhang et al. correlation [35] and Amalfi et al. correlation [32] forecasted a high level of the heating cost c_h and the payback time *PBT*. A high level of the carbon emission was obtained by the Zhang and Haglind correlation [34] or the Kuo et al. correlation [36]. The results would be helpful to picture out the true effect of the two-phase correlation selections on the heat pump performance assessment.

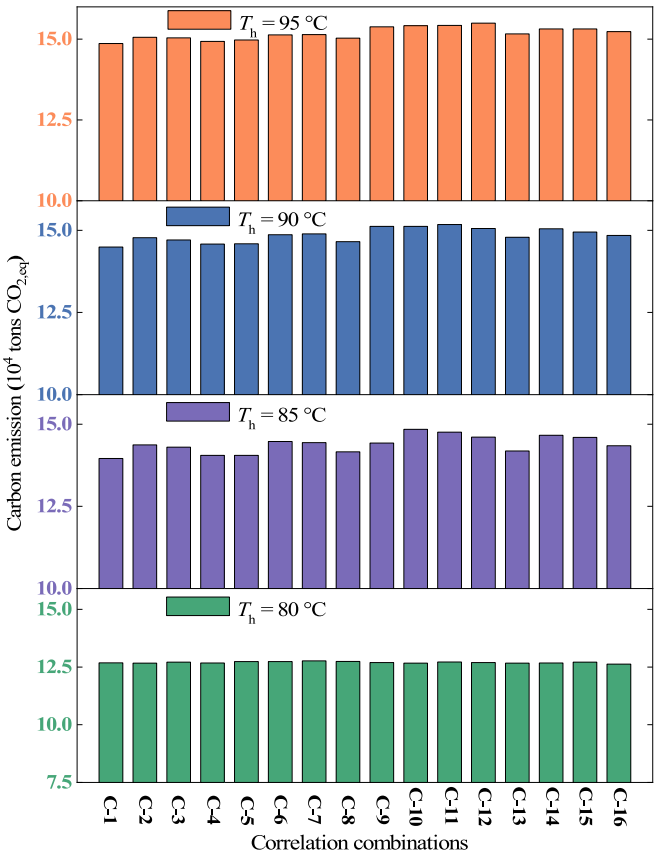

Fig. 21. Comparison of system carbon emissions under various T_h.

CRediT authorship contribution statement

Ding Wu: Writing – original draft, Methodology, Formal analysis, Conceptualization. **Bo Ma:** Writing – review & editing, Supervision, Funding acquisition, Formal analysis, Conceptualization. **Xiaohui Huang:** Writing – review & editing, Formal analysis. **Xian Wu:** Writing – review & editing, Formal analysis. **Yan Yang:** Writing – review & editing, Methodology, Formal analysis. **Chuang Wen:** Writing – review & editing, Supervision, Methodology, Funding acquisition, Formal analysis, Conceptualization. **Ji Zhang:** Writing – review & editing, Supervision, Funding acquisition, Formal analysis, Conceptualization.

Declaration of competing interest

The authors declare that they have no known competing financial interests or personal relationships that could have appeared to influence the work reported in this paper.

Acknowledgments

This work was supported in part by the National Natural Science Foundation of China under Grant 52377047, the Disaster Prevention & Reduction Center of State Grid Hunan Corporation (Grant No. SGHNFZ00JLJS2400035), and the Engineering and Physical Sciences Research Council [grant number EP/Y022149/1]. For the purpose of open access, the author has applied a 'Creative Commons Attribution (CC BY) licence to any Author Accepted Manuscript version arising.

Data availability

Data will be made available on request.

References

[1] Jayakumar M, Bizuneh Gebeyehu K, Deso Abo L, Wondimu Tadesse A, Vivekanandan B, Prabhu Sundramurthy V, et al. A comprehensive outlook on topical processing methods for biofuel production and its thermal applications: current advances, sustainability and challenges. Fuel 2023;349:128690. https://doi.org/10.1016/j.fuel.2023.128690.
[2] Kim H, Junghans L. Economic feasibility of achieving net-zero emission building (NZEB) by applying solar and geothermal energy sources to heat pump systems: a case in the United States residential sector. J Clean Prod 2023;416:137822. https://doi.org/10.1016/j.jclepro.2023.137822.
[3] Agency IE. Net zero by 2050: A roadmap for the global energy sector. 4 ed. Paris: OECD Publishing; 2021. https://doi.org/10.1787/c8328405-en.
[4] Kim M-H, Kim D-W, Lee D-W, Heo J. Energy conservation performance of a solar thermal and seasonal thermal energy storage-based renewable energy convergence system for glass greenhouses. Case Studies Thermal Eng 2023;44:102895. https://doi.org/10.1016/j.csite.2023.102895.
[5] Stolarski MJ, Warmiński K, Krzyżaniak M, Olba–Ziety E, Stachowicz P. Energy consumption and heating costs for a detached house over a 12-year period – renewable fuels versus fossil fuels. Energy 2020;204:117952. https://doi.org/10.1016/j.energy.2020.117952.
[6] Yang D, Huo Y, Zhang Q, Xie J, Yang Z. Recent advances on air heating system of cabin for pure electric vehicles: a review. Heliyon 2022;8:e11032. https://doi.org/10.1016/j.heliyon.2022.e11032.
[7] Galvin R. Policy pressure to retrofit Germany's residential buildings to higher energy efficiency standards: a cost-effective way to reduce CO2 emissions? Build Environ 2023;237:110316. https://doi.org/10.1016/j.buildenv.2023.110316.
[8] Yıldız Ç, Seçilmiş M, Arıcı M, Mert MS, Nižetić S, Karabay H. An experimental study on a solar-assisted heat pump incorporated with PCM based thermal energy storage unit. Energy 2023;278:128035. https://doi.org/10.1016/j.energy.2023.128035.
[9] Jahangir MH, Labbafi S. Optimization of ground source heat pump system along with energy storage tank armed with phase change materials to improve the microalgae open culture system performance. J Energy Storage 2022;51:104436. https://doi.org/10.1016/j.est.2022.104436.
[10] Su Z, Zhang M, Xu P, Zhao Z, Wang Z, Huang H, et al. Opportunities and strategies for multigrade waste heat utilization in various industries: a recent review. Energ Conver Manage 2021;229:113769. https://doi.org/10.1016/j.enconman.2020.113769.
[11] Walden JVM, Bähr M, Glade A, Gollasch J, Tran AP, Lorenz T. Nonlinear operational optimization of an industrial power-to-heat system with a high temperature heat pump, a thermal energy storage and wind energy. Appl Energy 2023;344:121247. https://doi.org/10.1016/j.apenergy.2023.121247.
[12] Wang Y, Quan Z, Zhao Y, Wang L, Jing H. Operation mode performance and optimization of a novel coupled air and ground source heat pump system with energy storage: case study of a hotel building. Renew Energy 2022;201:889–903. https://doi.org/10.1016/j.renene.2022.11.016.
[13] Yang X, Sun D, Li J, Yu C, Deng Y, Yu B. Demonstration study on ground source heat pump heating system with solar thermal energy storage for greenhouse heating. J Energy Storage 2022;54:105298. https://doi.org/10.1016/j.est.2022.105298.
[14] Du K, Calautit J, Eames P, Wu Y. A state-of-the-art review of the application of phase change materials (PCM) in mobilized-thermal energy storage (M-TES) for recovering low-temperature industrial waste heat (IWH) for distributed heat supply. Renew Energy 2021;168:1040–57. https://doi.org/10.1016/j.renene.2020.12.057.
[15] Schellenberg C, Lohan J, Dimache L. Comparison of metaheuristic optimisation methods for grid-edge technology that leverages heat pumps and thermal energy storage. Renew Sustain Energy Rev 2020;131:109966. https://doi.org/10.1016/j.rser.2020.109966.
[16] Zhang S, Ocłoń P, Klemeš JJ, Michorczyk P, Pielichowska K, Pielichowski K. Renewable energy systems for building heating, cooling and electricity production with thermal energy storage. Renew Sustain Energy Rev 2022;165:112560. https://doi.org/10.1016/j.rser.2022.112560.
[17] Lee DY, Seo BM, Hong SH, Choi JM, Lee KH. Part load ratio characteristics and energy saving performance of standing column well geothermal heat pump system assisted with storage tank in an apartment. Energy 2019;174:1060–78. https://doi.org/10.1016/j.energy.2019.03.029.
[18] Sakellariou EI, Wright AJ, Axaopoulos P, Oyinlola MA. PVT based solar assisted ground source heat pump system: modelling approach and sensitivity analyses. Solar Energy 2019;193:37–50. https://doi.org/10.1016/j.solener.2019.09.044.
[19] Fernández-Seara J, Pereiro A, Bastos S, Dopazo JA. Experimental evaluation of a geothermal heat pump for space heating and domestic hot water simultaneous production. Renew Energy 2012;48:482–8. https://doi.org/10.1016/j.renene.2012.05.019.
[20] Liu D-x, Lei H-Y, Li J-S, Dai C-s, Xue R, Liu X. Optimization of a district heating system coupled with a deep open-loop geothermal well and heat pumps. Renew Energy 2024;223:119991. https://doi.org/10.1016/j.renene.2024.119991.
[21] Marinelli S, Lolli F, Butturi MA, Rimini B, Gamberini R. Environmental performance analysis of a dual-source heat pump system. Energ Buildings 2020;223:110180. https://doi.org/10.1016/j.enbuild.2020.110180.
[22] Osterman E, Stritih U. Review on compression heat pump systems with thermal energy storage for heating and cooling of buildings. J Energy Storage 2021;39:102569. https://doi.org/10.1016/j.est.2021.102569.
[23] Vannoni A, Sorce A, Traverso A, Fausto Massardo A. Techno-economic optimization of high-temperature heat pumps for waste heat recovery. Energ

Conver Manage 2023;290:117194. https://doi.org/10.1016/j.enconman.2023.117194.
[24] Sim J, Lee H, Jeong JH. Optimal design of variable-path heat exchanger for energy efficiency improvement of air-source heat pump system. Appl Energy 2021;290:116741. https://doi.org/10.1016/j.apenergy.2021.116741.
[25] Mancini R, Zühlsdorf B, Aute V, Markussen WB, Elmegaard B. Performance of heat pumps using pure and mixed refrigerants with maldistribution effects in plate heat exchanger evaporators. Int J Refrigeration 2019;104:390–403. https://doi.org/10.1016/j.ijrefrig.2019.05.023.
[26] Abou Elmaaty TM, Kabeel AE, Mahgoub M. Corrugated plate heat exchanger review. Renew Sustain Energy Rev 2017;70:852–60. https://doi.org/10.1016/j.rser.2016.11.266.
[27] Cattelan G, Diani A, Azzolin M. Condensation heat transfer of R1234ze(E) and R134a inside a brazed plate heat exchanger: experimental data and model assessment. Int J Refrigeration 2022;143:57–67. https://doi.org/10.1016/j.ijrefrig.2022.06.022.
[28] Eldeeb R, Aute V, Radermacher R. A survey of correlations for heat transfer and pressure drop for evaporation and condensation in plate heat exchangers. Int J Refrigeration 2016;65:12–26. https://doi.org/10.1016/j.ijrefrig.2015.11.013.
[29] Liu Z, Winterton RHS. A general correlation for saturated and subcooled flow boiling in tubes and annuli, based on a nucleate pool boiling equation. Int J Heat Mass Transfer 1991;34:2759–66. https://doi.org/10.1016/0017-9310(91)90234-6.
[30] Tao X, Infante Ferreira CA. Heat transfer and frictional pressure drop during condensation in plate heat exchangers: assessment of correlations and a new method. Int J Heat Mass Transfer 2019;135:996–1012. https://doi.org/10.1016/j.ijheatmasstransfer.2019.01.132.
[31] Shah MM. Heat transfer during condensation in corrugated plate heat exchangers. Int J Refrigeration 2021;127:180–93. https://doi.org/10.1016/j.ijrefrig.2021.02.011.
[32] Amalfi RL, Vakili-Farahani F, Thome JR. Flow boiling and frictional pressure gradients in plate heat exchangers. Part 2: comparison of literature methods to database and new prediction methods. Int J Refrigeration 2016;61:185–203. https://doi.org/10.1016/j.ijrefrig.2015.07.009.
[33] Yan Y, Lin T. Evaporation heat transfer and pressure drop of refrigerant R-134a in a plate heat exchanger. J Heat Transfer-Transactions ASME 1999;121:118–27.
[34] Zhang J, Haglind F. Experimental analysis of high temperature flow boiling heat transfer and pressure drop in a plate heat exchanger. Appl Therm Eng 2021;196:117269. https://doi.org/10.1016/j.applthermaleng.2021.117269.
[35] Zhang J, Kærn MR, Ommen T, Elmegaard B, Haglind F. Condensation heat transfer and pressure drop characteristics of R134a, R1234ze(E), R245fa and R1233zd(E) in a plate heat exchanger. Int J Heat Mass Transfer 2019;128:136–49. https://doi.org/10.1016/j.ijheatmasstransfer.2018.08.124.
[36] Kuo WS, Lie YM, Hsieh YY, Lin TF. Condensation heat transfer and pressure drop of refrigerant R-410A flow in a vertical plate heat exchanger. Int J Heat Mass Transfer 2005;48:5205–20. https://doi.org/10.1016/j.ijheatmasstransfer.2005.07.023.
[37] Han D-H, Lee K-J, Kim Y-H. The characteristics of condensation in brazed plate heat exchangers with different chevron angles. J-Korean Phys Soc 2003;43:66–73.
[38] Yan Y-Y, Lio H-C, Lin T-F. Condensation heat transfer and pressure drop of refrigerant R-134a in a plate heat exchanger. Int J Heat Mass Transfer 1999;42:993–1006. https://doi.org/10.1016/S0017-9310(98)00217-8.
[39] Kim B, Lee D, Lee SH, Kim Y. Performance assessment of optimized heat pump water heaters using low-GWP refrigerants for high- and low-temperature applications. Appl Therm Eng 2020;181:115954. https://doi.org/10.1016/j.applthermaleng.2020.115954.
[40] Salazar-Herran E, Martin-Escudero K, Alleyne AG, del Portillo-Valdes LA, Romero-Anton N. Numerical model for liquid-to-liquid heat pumps implementing switching mode. Appl Therm Eng 2019;160:114054. https://doi.org/10.1016/j.applthermaleng.2019.114054.
[41] Yan H, Wu D, Liang J, Hu B, Wang RZ. Selection and validation on low-GWP refrigerants for a water-source heat pump. Appl Therm Eng 2021;193:116938. https://doi.org/10.1016/j.applthermaleng.2021.116938.
[42] Zhao X, Huang S, Xie N, Wang L, Li H. Simultaneous optimization of working fluid and temperature matching for heat pump assisted geothermal cascade heating system. Case Studies Thermal Eng 2023;41:102685. https://doi.org/10.1016/j.csite.2022.102685.
[43] Fischer D, Bernhardt J, Madani H, Wittwer C. Comparison of control approaches for variable speed air source heat pumps considering time variable electricity prices and PV. Appl Energy 2017;204:93–105. https://doi.org/10.1016/j.apenergy.2017.06.110.
[44] Lee S, Chung Y, Kim S, Jeong Y, Kim MS. Predictive optimization method for the waste heat recovery strategy in an electric vehicle heat pump system. Appl Energy 2023;333:120572. https://doi.org/10.1016/j.apenergy.2022.120572.
[45] Lee S, Chung Y, Jeong Y, Kim MS. Investigation on the performance enhancement of electric vehicle heat pump system with air-to-air regenerative heat exchanger in cold condition. Sustain Energy Technol Assess 2022;50:101791. https://doi.org/10.1016/j.seta.2021.101791.
[46] Zhang N, Lu Y, Kadam S, Yu Z. Investigation of the integrated fuel cell, battery, and heat pump energy systems. Energ Conver Manage 2023;276:116503. https://doi.org/10.1016/j.enconman.2022.116503.
[47] Ommen T, Jensen JK, Markussen WB, Reinholdt L, Elmegaard B. Technical and economic working domains of industrial heat pumps: part 1 – single stage vapour compression heat pumps. Int J Refrigeration 2015;55:168–82. https://doi.org/10.1016/j.ijrefrig.2015.02.012.
[48] Kosmadakis G, Neofytou P. Reversible high-temperature heat pump/ORC for waste heat recovery in various ships: a techno-economic assessment. Energy 2022;256:124634. https://doi.org/10.1016/j.energy.2022.124634.
[49] Zanetti E, Bonduà S, Bortolin S, Bortolotti V, Azzolin M, Tinti F. Sequential coupled numerical simulations of an air/ground-source heat pump: validation of the model and results of yearly simulations. Energ Buildings 2022;277:112540. https://doi.org/10.1016/j.enbuild.2022.112540.
[50] Dai B, Feng Y, Liu S, Yao X, Zhang J, Wang B, et al. Dual pressure condensation heating high temperature heat pump using eco-friendly working fluid mixtures for industrial heating processes: 4E analysis. Energy 2023;283:128639. https://doi.org/10.1016/j.energy.2023.128639.
[51] Pelella F, Zsembinszki G, Viscito L, William Mauro A, Cabeza LF. Thermo-economic optimization of a multi-source (air/sun/ground) residential heat pump with a water/PCM thermal storage. Appl Energy 2023;331:120398. https://doi.org/10.1016/j.apenergy.2022.120398.
[52] Le AT, Wang L, Wang Y, Li D. Measurement investigation on the feasibility of shallow geothermal energy for heating and cooling applied in agricultural greenhouses of Shouguang City: ground temperature profiles and geothermal potential. Info Processing Agri 2021;8:251–69. https://doi.org/10.1016/j.inpa.2020.06.001.
[53] Wang Y, Li C, Zhao J, Wu B, Du Y, Zhang J, et al. The above-ground strategies to approach the goal of geothermal power generation in China: state of art and future researches. Renew Sustain Energy Rev 2021;138:110557. https://doi.org/10.1016/j.rser.2020.110557.
[54] Zühlsdorf B, Jensen JK, Elmegaard B. Heat pump working fluid selection—economic and thermodynamic comparison of criteria and boundary conditions. Int J Refrigeration 2019;98:500–13. https://doi.org/10.1016/j.ijrefrig.2018.11.034.
[55] Sarbu I. Heat pumps for sustainable heating and cooling. Advances in building services engineering: Studies, researches and applications. Germany: Springer Cham; 2021. p. 447–557.
[56] Abu-Rayash A, Dincer I. Development of an integrated energy system for smart communities. Energy 2020;202:117683. https://doi.org/10.1016/j.energy.2020.117683.
[57] Fadaei A, Noorollahi Y, Pakzad P, Yousefi H. Development, 4E-analysis, and optimization of a seawater thermal energy-driven desalination system based on seawater source heat pump, multi-effect desalination, and pressure retarded osmosis with reduced effluent concentration. Energ Conver Manage 2023;298:117746. https://doi.org/10.1016/j.enconman.2023.117746.
[58] Deb K, Pratap A, Agarwal S, Meyarivan T. A fast and elitist multiobjective genetic algorithm: NSGA-II. IEEE Trans Evolutionary Comput 2002;6:182–97. https://doi.org/10.1109/4235.996017.
[59] Wu D, Hu B, Wang RZ. Vapor compression heat pumps with pure low-GWP refrigerants. Renew Sustain Energy Rev 2021;138:110571. https://doi.org/10.1016/j.rser.2020.110571.
[60] Heredia-Aricapa Y, Belman-Flores JM, Mota-Babiloni A, Serrano-Arellano J, García-Pabón JJ. Overview of low GWP mixtures for the replacement of HFC refrigerants: R134a, R404A and R410A. Int J Refrigeration 2020;111:113–23. https://doi.org/10.1016/j.ijrefrig.2019.11.012.
[61] Abedini H, Vieren E, Demeester T, Beyne W, Lecompte S, Quoilin S, et al. A comprehensive analysis of binary mixtures as working fluid in high temperature heat pumps. Energ Conver Manage 2023;277:116652. https://doi.org/10.1016/j.enconman.2022.116652.
[62] İşkan Ü, Direk M. Experimental performance evaluation of the dual-evaporator ejector refrigeration system using environmentally friendly refrigerants of R1234ze(E), ND, R515a, R456a, and R516a as a replacement for R134a. J Clean Prod 2022;352:131612. https://doi.org/10.1016/j.jclepro.2022.131612.
[63] Wang S, Liu C, Zhang S, Li Q, Huo E. Multi-objective optimization and fluid selection of organic Rankine cycle (ORC) system based on economic-environmental-sustainable analysis. Energ Conver Manage 2022;254:115238. https://doi.org/10.1016/j.enconman.2022.115238.
[64] Jin X, Zhang J, Liu Z, Hong W, Sha S, Qiu Z, et al. Performance analysis of a two-stage vapor compression heat pump based on intercooling effect. Case Studies Thermal Eng 2023;51:103643. https://doi.org/10.1016/j.csite.2023.103643.
[65] Wang Y, Nan X, Ouyang H, Guo Z, Hu B, Wang RZ. Analysis and optimization of injection characteristics and comprehensive performance of low GWP refrigerant HP-1 in high temperature heat pump systems. Energ Buildings 2024;303:113799. https://doi.org/10.1016/j.enbuild.2023.113799.
[66] Arsenyeva O, Tovazhnyanskyy L, Kapustenko P, Klemeš JJ, Varbanov PS. Review of developments in plate heat exchanger heat transfer enhancement for single-phase applications in process industries. Energies 2023. https://doi.org/10.3390/en16134976.
[67] Imran M, Usman M, Park B-S, Yang Y. Comparative assessment of organic Rankine cycle integration for low temperature geothermal heat source applications. Energy 2016;102:473–90. https://doi.org/10.1016/j.energy.2016.02.119.
[68] Kumar S, Singh SK, Sharma D. A comprehensive review on thermal performance enhancement of plate heat exchanger. Int J Thermophys 2022;43:109. https://doi.org/10.1007/s10765-022-03036-7.
[69] Zhang J, Hu X, Wu D, Huang X, Wang X, Yang Y, et al. A comparative study on design and performance evaluation of organic Rankine cycle (ORC) under different two-phase heat transfer correlations. Appl Energy 2023;350:121724. https://doi.org/10.1016/j.apenergy.2023.121724.
[70] Zhang J, Desideri A, Kærn MR, Ommen TS, Wronski J, Haglind F. Flow boiling heat transfer and pressure drop characteristics of R134a, R1234yf and R1234ze in a plate heat exchanger for organic Rankine cycle units. Int J Heat Mass Transfer 2017;108:1787–801. https://doi.org/10.1016/j.ijheatmasstransfer.2017.01.026.

[71] Xu J, Luo X, Chen Y, Mo S. Multi-criteria design optimization and screening of heat exchangers for a subcritical ORC. Energy Procedia 2015;75:1639–45. https://doi.org/10.1016/j.egypro.2015.07.397.
[72] Bao J, Zhao L. A review of working fluid and expander selections for organic Rankine cycle. Renew Sustain Energy Rev 2013;24:325–42. https://doi.org/10.1016/j.rser.2013.03.040.
[73] Cooper MG. Saturation nucleate pool boiling - A simple correlation. In: Simpson HC, Hewitt GF, Boland D, Bott TR, Furber BN, Hall WB, et al., editors. First UK National Conference on Heat Transfer: Pergamon; 1984. p. 785–93.
[74] Annaratone D. Introduction to heat transfer. In: Annaratone D, editor. Engineering heat transfer. Berlin, Heidelberg: Springer Berlin Heidelberg; 2010. p. 1–11.
[75] Hsieh YY, Lin TF. Saturated flow boiling heat transfer and pressure drop of refrigerant R-410A in a vertical plate heat exchanger. Int J Heat Mass Transfer 2002;45:1033–44. https://doi.org/10.1016/S0017-9310(01)00219-8.
[76] Würfel R, Ostrowski N. Experimental investigations of heat transfer and pressure drop during the condensation process within plate heat exchangers of the herringbone-type. Int J Thermal Sci 2004;43:59–68. https://doi.org/10.1016/S1290-0729(03)00099-1.
[77] Akers WW, Deans HA, Crosser OK. Condensation heat transfer within horizontal tubes. Chem Eng Progr Symp Ser 1959;55:171–6. http://refhub.elsevier.com/S0017-9310(18)31996-3/h0220.
[78] Longo GA, Righetti G, Zilio C. A new computational procedure for refrigerant condensation inside herringbone-type brazed plate heat exchangers. Int J Heat Mass Transfer 2015;82:530–6. https://doi.org/10.1016/j.ijheatmasstransfer.2014.11.032.
[79] Lu P, Luo X, Wang J, Chen J, Liang Y, Yang Z, et al. Thermo-economic design, optimization, and evaluation of a novel zeotropic ORC with mixture composition adjustment during operation. Energ Conver Manage 2021;230:113771. https://doi.org/10.1016/j.enconman.2020.113771.
[80] Liu C, Gao T. Off-design performance analysis of basic ORC, ORC using zeotropic mixtures and composition-adjustable ORC under optimal control strategy. Energy 2019;171:95–108. https://doi.org/10.1016/j.energy.2018.12.195.
[81] Martin H. A theoretical approach to predict the performance of chevron-type plate heat exchangers. Chem Eng Processing: Process Intensific 1996;35:301–10. https://doi.org/10.1016/0255-2701(95)04129-X.
[82] Usman M, Imran M, Yang Y, Lee DH, Park B-S. Thermo-economic comparison of air-cooled and cooling tower based organic Rankine cycle (ORC) with R245fa and R1233zde as candidate working fluids for different geographical climate conditions. Energy 2017;123:353–66. https://doi.org/10.1016/j.energy.2017.01.134.
[83] Çakır U, Çomaklı K. Exergetic interrelation between an heat pump and components. Appl Therm Eng 2016;105:659–68. https://doi.org/10.1016/j.applthermaleng.2016.03.062.
[84] Hu X, Liu Y, Dong S, Li G, Sun Z, Liu Y. Comparison study of conventional and advanced exergy analysis on cascade high temperature heat pump system based on experiment. Case Studies Thermal Eng 2022;40:102552. https://doi.org/10.1016/j.csite.2022.102552.
[85] Lu Z, Yao Y, Liu G, Ma W, Gong Y. Thermodynamic and economic analysis of a high temperature Cascade heat pump system for steam generation. Processes 2022;10:1862.
[86] Bühler F, Zühlsdorf B, Nguyen T-V, Elmegaard B. A comparative assessment of electrification strategies for industrial sites: case of milk powder production. Appl Energy 2019;250:1383–401. https://doi.org/10.1016/j.apenergy.2019.05.071.
[87] Dai B, Wang Q, Liu S, Wang D, Yu L, Li X, et al. Novel configuration of dual-temperature condensation and dual-temperature evaporation high-temperature heat pump system: carbon footprint, energy consumption, and financial assessment. Energ Conver Manage 2023;292:117360. https://doi.org/10.1016/j.enconman.2023.117360.
[88] Fukuda S, Kondou C, Takata N, Koyama S. Low GWP refrigerants R1234ze(E) and R1234ze(Z) for high temperature heat pumps. Int J Refrigeration 2014;40:161–73. https://doi.org/10.1016/j.ijrefrig.2013.10.014.
[89] Baral AA, Minjares R. Upstream climate impacts from production of R-134a and R-1234yf refrigerants used in mobile air conditioning systems. 2025.
[90] Yang C, Seo S, Takata N, Thu K, Miyazaki T. The life cycle climate performance evaluation of low-GWP refrigerants for domestic heat pumps. Int J Refrigeration 2021;121:33–42. https://doi.org/10.1016/j.ijrefrig.2020.09.020.
[91] Wang Z, Wang F, Wang X, Ma Z, Wu X, Song M. Dynamic character investigation and optimization of a novel air-source heat pump system. Appl Therm Eng 2017;111:122–33. https://doi.org/10.1016/j.applthermaleng.2016.09.076.
[92] Kavian S, Aghanajafi C, Dizadji N. Transient simulation and multi-objective optimization of a VSD ground source heat pump in various usage. Energ Conver Manage 2019;197:111847. https://doi.org/10.1016/j.enconman.2019.111847.
[93] Zhu T, Ommen T, Meesenburg W, Thorsen JE, Elmegaard B. Steady state behavior of a booster heat pump for hot water supply in ultra-low temperature district heating network. Energy 2021;237:121528. https://doi.org/10.1016/j.energy.2021.121528.
[94] Mete Ozturk M, Doğan B, Berrin Erbay L. Performance assessment of an air source heat pump water heater from exergy aspect. Sustain Energy Technol Assess 2020;42:100809. https://doi.org/10.1016/j.seta.2020.100809.
[95] Lee M, Kim J, Shin HH, Cho W, Kim Y. CO2 emissions and energy performance analysis of ground-source and solar-assisted ground-source heat pumps using low-GWP refrigerants. Energy 2022;261:125198. https://doi.org/10.1016/j.energy.2022.125198.